Through a glass darkly: improving raypath interferometry

David C. Henley

ABSTRACT

The processing technique known as raypath interferometry has been successfully applied to several different sets of 3C model and field seismic data, to correct their images for degradation caused by irregularities in the near-surface layer. We continue to refine and improve the technique. In this report, we demonstrate an alternative scheme for creating the reference wavefield, or 'pilot traces' used in the interferometry, and we demonstrate the use of the Snell Transform, a modified Radial Trace Transform, for mapping the raw seismic data into the common-raypath domain required by raypath interferometry.

For pilot trace creation from raw data gathers, we find that singular value decomposition (SVD) methods can be used as an alternate or supplement to lateral smoothing, but that this method, like lateral smoothing, operates best when lateral structure and discontinuities are first reduced by 'brute force' techniques like horizon flattening and 'trim' statics.

The Snell Transform, because its sampling trajectories are more likely to map seismic data at all depths onto common raypaths, appears to lead to slightly better interferometric images, especially at shallow depths, than the Radial Trace Transform; but trial and error are needed to set parameters appropriately.

INTRODUCTION

Interferometry instead of trace shifting

Interferometry is a family of wave propagation techniques widely used in the physical sciences to perform imaging or image corrections, or to characterize the media through which waves are propagated. Over the past few years, we have developed a processing technique, based partly on interferometric principles, that allows us to correct seismic data for the image disturbances caused by the irregularities of the near-surface layer. This technique, called 'raypath interferometry', was developed as an alternative to conventional residual statics methods, and generalizes some of the more restrictive assumptions required by those methods. This enables raypath interferometry to deal with near-surface conditions which clearly violate residual statics assumptions, like high-velocity surface layers, multi-path reflection arrivals, and non-stationary statics (Henley, 2012a). All of the above were encountered during the first successful application of the method to field seismic data in the MacKenzie Delta (Henley, 2012a), and it was this example, as well, that highlighted the importance of the pilot trace creation process for this particular form of interferometry.

Most forms of seismic interferometry are based on cross-correlations of pairs of raw seismic traces (Bakulin and Calvert, 2006), which are summed over common surface location and used to estimate the Green's Function corresponding to that location. We, on the other hand, take an alternate approach, more akin to simple optical interferometry, in

which we sum raw traces, *then* correlate the sum with individual raw traces. The individual correlation functions can be used either as matched filters to correct their corresponding raw traces by correlation, or they can be used to derive inverse filters to correct the corresponding traces by convolution. By carefully controlling the raw trace summation process (summing along reflecting horizons and force-aligning adjacent traces), the summation gives a good estimate of the propagating signal waveform. Underlying lateral geological variations are averaged out by the process, thus simulating an undisturbed 'reference wavefield', as used in optical interferometry (see Figure 1). In this figure, the passage of undisturbed wavefronts through a uniform medium represents the process whereby we estimate the seismic reference wavefield by conditioning and smoothing raw seismic traces (described later). Correlating raw traces with the traces of the reference wavefield produces cross-correlations or 'surface functions' which contain timing and phase information primarily associated with the surface locations of the raw traces. Hence, using the surface functions as matched filters, or, preferably, using them to derive broadband inverse filters, constitutes our use of interferometry to apply surface corrections to seismic traces. Because we use the entire cross-correlation function, we can apply not only a bulk shift (static correction), but the phase adjustments implied by complexity in the reflection arrival waveform (multi-path arrivals, scattered arrivals). The inverse filter applied to each seismic trace not only shifts it into approximate alignment with the reference wavefield, but simplifies its waveform by collapsing any complicated pattern of arrivals into a single arrival.

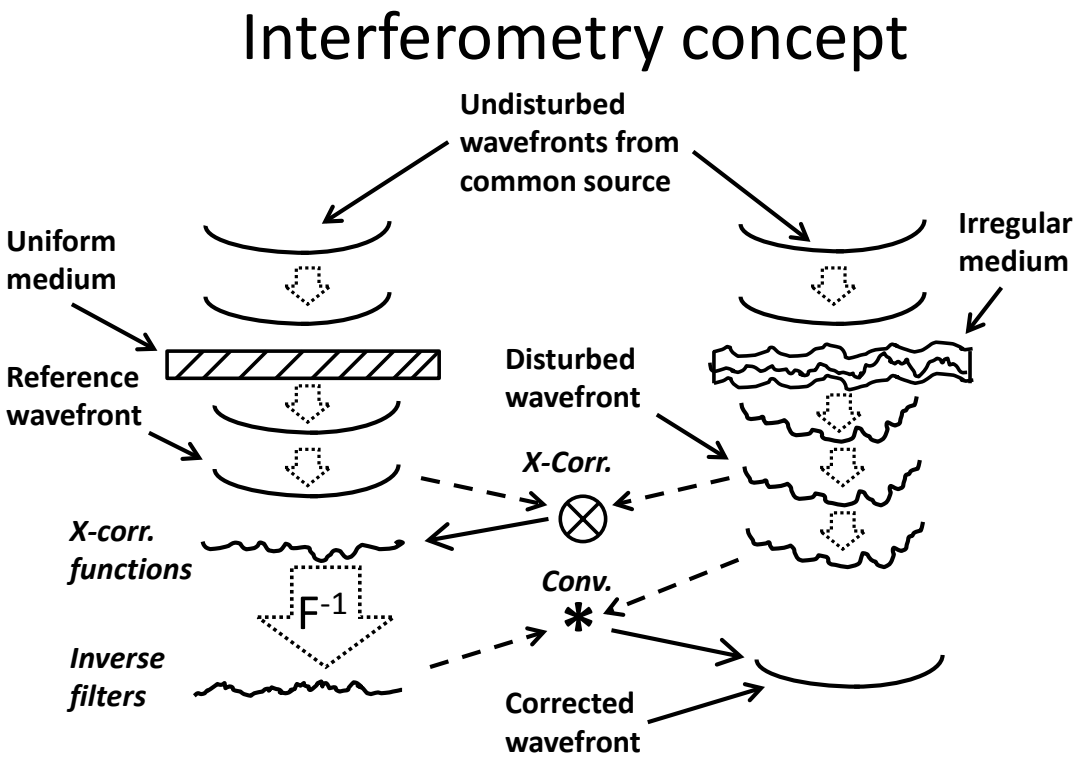

FIG.1. Schematic showing the optical interferometry concept adapted for use in Raypath Interferometry. The first part of the path on the left becomes the process of generating 'pilot traces' in the Raypath Interferometry procedure.

Clearly, the construction of the reference wavefield used for the interferometry process is of key importance to the success of its operation. As with most complex problems with many variables, in which we seek to minimize some measurement of error, this particular form of interferometry performs best when the starting point is close to the solution point. In this case, the more nearly the starting reference wavefield resembles the wavefield after interferometric correction, the better the results. Likewise, as with most similar techniques, the interferometry process can be iterated; the corrected traces from the first iteration can be summed to form a reference wavefield for a second round of cross-correlation and inverse filter derivation, and so forth. We have investigated the sensitivity of the reference wavefield estimate to our artificial forcing; in some cases summing the raw traces laterally, instead of following geological structure (requiring picking a horizon) for long-wavelength alignment, and in other cases omitting the 'trim static' short-wavelength alignment. Experience has shown that for seismic data with mild structure and 'average' statics, the interferometric solution may require an additional iteration if the reference wavefield is not summed along structure or the traces not subjected to trim statics. The final image, however, is indistinguishable from that obtained when these additional techniques are used in constructing the reference wavefield. When the apparent magnitude of short wavelength statics, or the vertical variation of the reflection time structure within the lateral summation window exceeds the predominant wavelength of the seismic event wavelet, however, horizon-following and trim-statics generally need to be applied in order to avoid 'loop-skipping' in the interferometric image (equivalent to the solution settling into a local minimum).

Exploring other means of reference wavefield estimation is obviously appealing, if we can avoid some of the subjectivity arising from horizon picking. One possibility, suggested by M. Yedlin (Yedlin, 2012), and described in this report, is to use Singular Value Decomposition to discard the detail associated with the least significant (shortest wavelength) components of a seismic trace ensemble and hence smooth the ensemble to form a reference wavefield estimate.

Raypath-consistency instead of surface-consistency

The other departure of raypath interferometry from convention is the generalization of the surface-consistency constraint to 'raypath-consistency' to allow the technique to handle seismic data for which the irregularities of the near surface cause wavefront disturbances which are neither surface consistent, nor stationary (uniform in time). Regions where the velocity of the near-surface layer approaches or exceeds that of underlying sediments are notorious for yielding such data. We have previously shown examples of seismic data from such regions (Henley, 2004, 2012a, 2012b), as well as the raypath interferometric solution for one of them (Henley, 2012a). It has recently been shown by Cova et al (2013a) that another situation in which nonstationarity of statics can arise is the shear-wave leg of converted wave data, where the lateral displacement of the conversion point with depth leads to significant variation of the near-surface raypath angle of emerging shear waves. This circumstance has been observed and compensated both on model data (Cova et al, 2013b) and on field data (Henley, 2012a, 2012b).

As an interesting sidelight, data in which surface-consistency or stationarity have been violated have, in some cases, been satisfactorily corrected using conventional statics

methods; and we conjecture that in such cases, it is likely that some of the nonstationarity of the corrections has been accommodated by corresponding adjustments in residual normal moveout (NMO) at various depths in the data. Since components of residual NMO are not orthogonal to (linearly independent of) components of residual statics, it seems reasonable that some of the misfit of statics to the surface-consistent model can leak into residual NMO and hence be reduced by adjustments to local NMO velocities. This remains to be tested rigorously, but our field data example from Hussar (Henley, 2012b) is consistent with this conjecture. On this example, the conventional residual statics solution, including residual NMO corrections, improved reflection continuity more for deeper events. Raypath interferometry, on the other hand, increased event continuity at most depths, particularly the shallow events, which required larger statics, while using a single fixed NMO function.

Using the raypath-consistency concept requires transforming seismic data into a domain where amplitudes are a function of some near-surface raypath parameter. In all previous work, we have used the radial trace (RT) transform, because of its simplicity and fidelity of inversion. Because it is a simple geometric point-to-point mapping of seismic amplitudes from the domain of travel time and source-receiver offset to a domain of travel time and apparent velocity, it can be inverted exactly, depending upon the type of interpolation used.

Figure 2 shows a raypath schematic corresponding to a trace from a seismic source gather in the XT domain, where it can be seen that the near-surface angle of raypath segments decreases with the depth of the particular reflecting horizon. A raypath schematic for a trace in the constant-raypath domain is shown in Figure 3, where raypath angles in all layers are constant, regardless of the depth of the reflecting point. This means that amplitudes on a common-raypath trace gather are dependent upon travel time and near-surface raypath angle, just as we desire. In actuality, the schematic in Figure 3 is not quite what we get with the RT transform, since in the standard RT transform, trace samples on an input gather are extracted along trajectories of constant apparent velocity (or slowness, reciprocally). This implies a schematic more like that in Figure 4, where raypath angles are constant in all layers, but take no account of Snell refraction at interface boundaries. Regardless of the fact that such raypaths depart significantly from reality, we have found the RT transform and its parameterization of conventional seismic traces approximately into common-raypath traces to work quite well in actual practice. The raypath interferometry procedure operates on common-raypath trace gathers, formed by sorting the RT transforms of the input seismic trace gathers. They are analogous to common-offset gathers in the conventional XT domain.

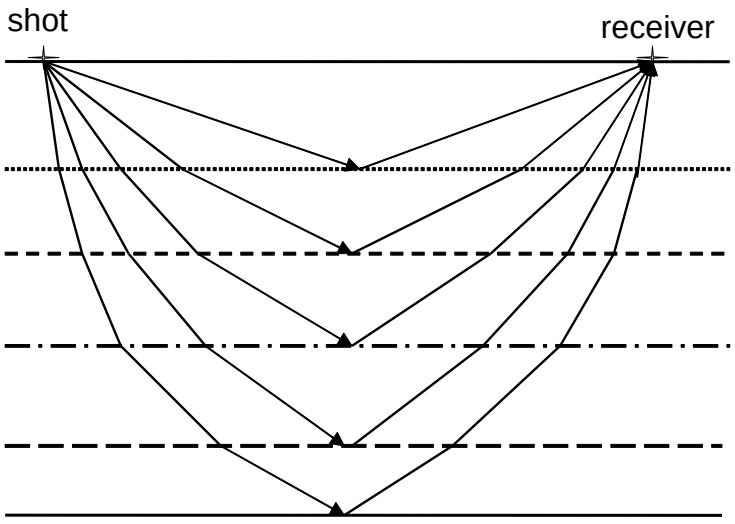

FIG. 2. Schematic diagram showing raypaths for different reflecting boundaries, as seen by a single seismic trace in the XT domain. The angles of incidence in all layers vary with the depth of the reflecting interface.

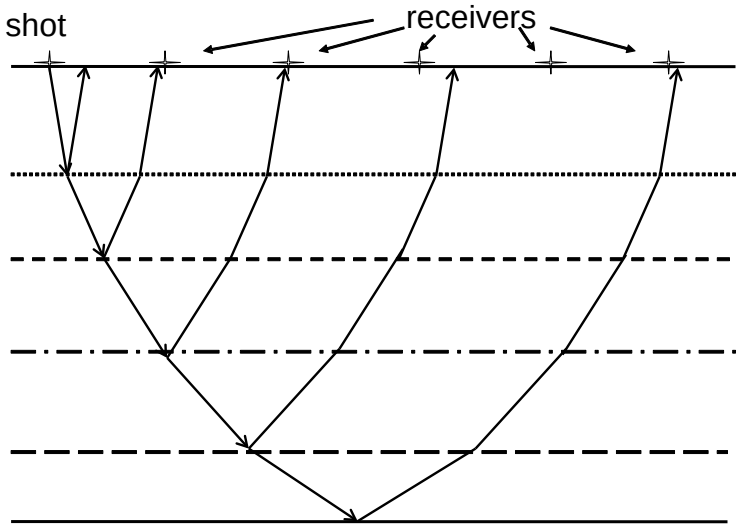

FIG. 3. Schematic diagram showing raypaths for a trace in the Snell Ray domain. Like the RT domain, incidence angles are constant in all layers regardless of the depth of the reflection, but unlike the RT domain, raypath segments obey Snell's law.

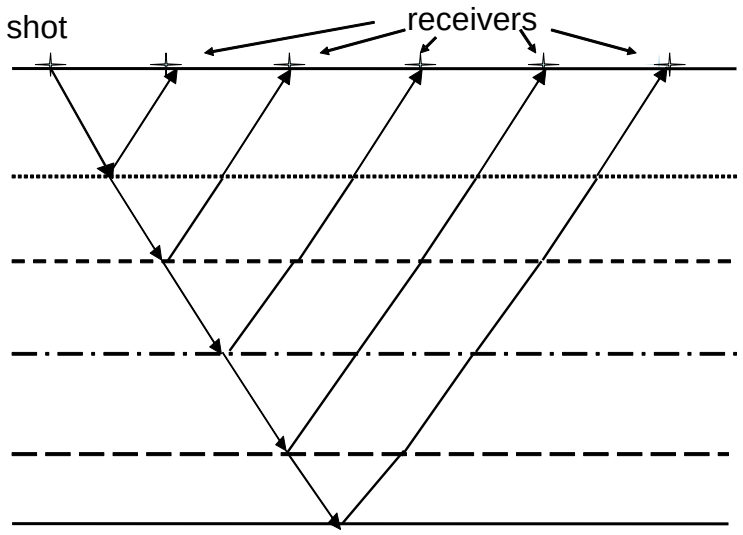

FIG. 4. Schematic diagram showing raypaths for a trace in the RT domain. While raypath incidence angles are constant in all layers, Snell's law is not obeyed at the interfaces.

An alternative to the standard radial trace transform exists, however: the 'Snell' transform, described by Claerbout (1975, 1985) and Ottolini (1982) in connection with the RT transform. In the Snell transform, the trajectories for sampling an input trace gather are bent or curved, rather than being linear, as in the RT transform. The bending or curvature is determined by the nominal interval velocity structure of the earth, so that each sampling trajectory approximately obeys Snell's law at each major reflecting boundary in the earth, thus approaching the raypath schematic in Figure 3. In this report we compare the Snell transform with the standard RT transform with respect to its effectiveness in the raypath interferometry application. We use field data for this comparison, while Cova et al (2014) demonstrate it on synthetic data as well as field data.

Another alternative to the RT transform, which was suggested by a query at a recent technical presentation on raypath interferometry is the Radon Transform, which also transforms input seismic trace gathers to a domain of travel time and ray parameter. We did not initially pursue this alternative because of invertibility issues with the Radon Transform. While in theory, a Radon Transform can be nearly exactly inverted as long as enough projections are constructed, spanning a wide enough aperture, in practice, because of aperture limitations the transform is considered "lossy" and loses some detail from the initial data set with each forward/inverse operation. Nevertheless, we consider this approach worthy of investigation, and some very encouraging results can be found in Cova et al (2014).

THE INVESTIGATION

The test data

In order to evaluate potential improvements to raypath interferometry, we chose to use simple image comparisons of stacked sections. For the comparisons, we chose two of the Hussar (Margrave et al, 2011) surveys: vertical component accelerometer with dynamite

source (PP), and radial component accelerometer with dynamite source (PS). The PP data set is attractive because its data quality is good and it has significant statics, which can be successfully corrected not only with raypath interferometry, but with conventional residual statics techniques, as well, making it a good standard test bed. By successfully applying raypath interferometry to these data, which do not violate surface-consistency, we confirmed that, because surface-consistency is just a special case of raypath-consistency (Henley, 2012b), raypath interferometry can be used for residual statics correction in general. Because its application is more tedious than conventional residual statics methods, however, its use is most appropriate for problem data sets where statics are large and possibly nonstationary, like converted wave surveys.

In the case of the Hussar PS data set, while it has been successfully corrected with conventional residual statics and NMO analysis, it exhibits substantial receiver statics (200ms) and displays evidence of nonstationarity, thus making it attractive for testing raypath interferometry.

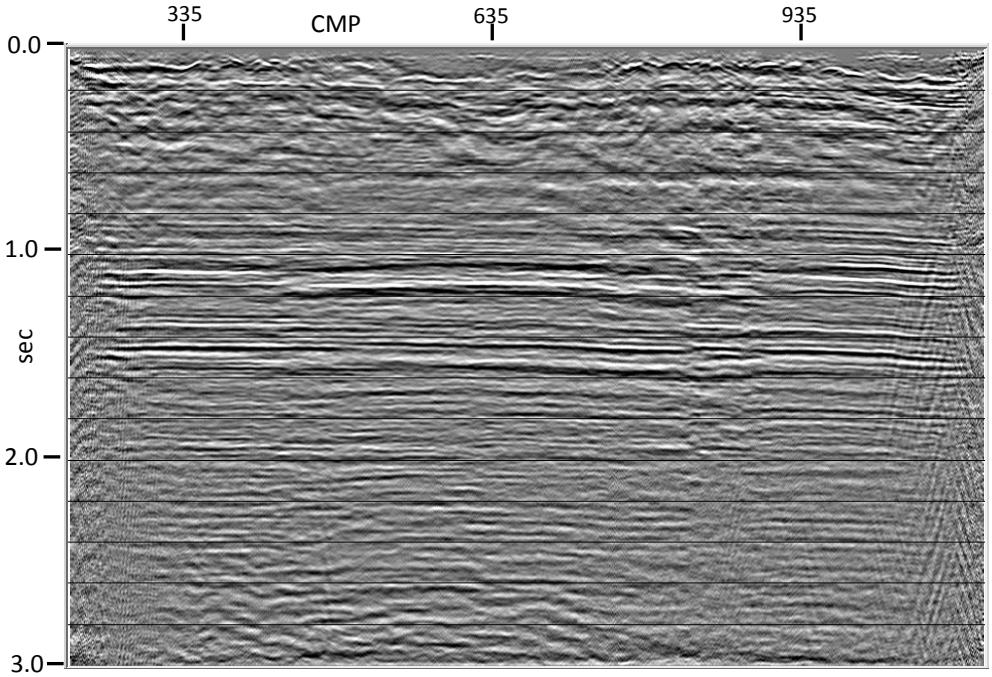

FIG. 5. Brute CMP stack of Hussar PP dynamite data using single NMO function—no statics applied.

Figure 5 shows the CMP stack of the Hussar PP data set that we used for all comparisons. The data represent the vertical component of the data set acquired with 3C accelerometers using dynamite sources. A single nominal NMO velocity function has been used for NMO correction, but no statics applied, and no deconvolution. AGC has been applied to scale the data for display. In this figure, the major reflection events are clearly visible, but their lateral continuity is obviously disturbed by the presence of unresolved near-surface disturbances. Radial trace filtering (Henley, 2003) was used to

remove source-generated noise from the source gathers, and consequently, no initial muting was applied. When the resulting gathers are NMO-corrected and CMP-stacked, the shallowest band of disturbed events, while likely not pure reflections, gives us some indication of the magnitude of the near-surface variations seen along the length of the 2D line. For all of our statics comparison tests, the RT-filtered source gathers were deconvolved using Gabor deconvolution, in order to normalize event amplitudes and whiten the spectrum. Figure 6 shows the result of applying conventional NMO analysis and residual statics to these data prior to CMP stacking. As can be seen from the event coherence, the near-surface irregularities have been well-compensated by the residual NMO and statics corrections. This figure provides the baseline comparison for all further results.

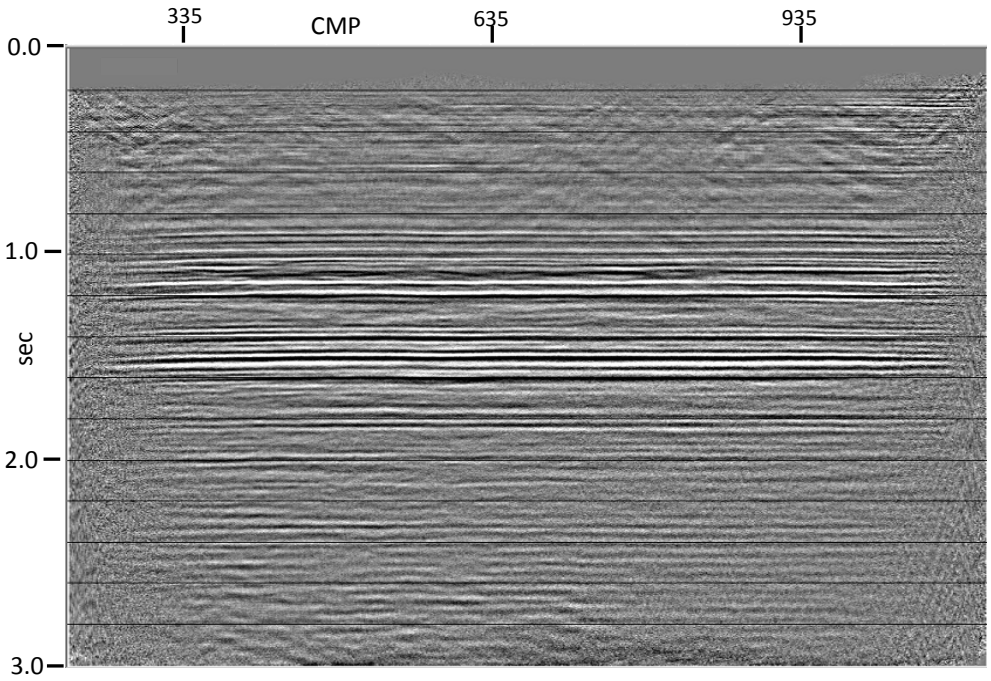

FIG. 6. CMP stack of Hussar PP dynamite data after NMO analysis and conventional residual statics are applied.

Constructing the reference wavefield

One of the keys to successful performance of the interferometric correction procedure used in raypath interferometry is the creation of a reference wavefield against which the raw traces of the input data are correlated to derive surface functions. In optical interferometry (Figure 1), the reference wavefield is simply the outgoing light wavefront, which has been transmitted through, at worst, a uniform medium, which does not disturb the phase or pulse shape along the wavefront. For seismic data, however, we never have an observation of the undisturbed outgoing wavefield (unless, perhaps in a deepwater marine environment), so we must improvise the reference wavefield in some heuristically defensible fashion. The reference wavefield is supposedly a representation of an outgoing wavefront which has the same pulse shape everywhere, and no local phase or timing disturbances. What we have from seismic data, however, are wavefronts convolved with

sequences of reflections and further disturbed by local timing and phase differences caused by the transit through the near-surface layer. How do we construct smooth, laterally homogeneous reference wavefields from such data without having already corrected the data for the very problem we are trying to address? The reflection sequences embedded in the data are not an issue, since in any correlation of raw traces with reference traces, the reflection sequences will be common and contribute no net phase components to the correlation functions. The reference traces should, however, contain little or no residual from the near-surface-induced time delays or wavelet shape differences caused by scattering or multipathing.

The most obvious technique for creating a reference wavefield from an ensemble of raw seismic traces is simply to smooth them laterally, a process usually known as trace mixing. If the reflections in the ensemble are horizontal, and the trace-to-trace shifts due to near-surface effects are relatively small, a simple trace mix can provide a useful set of reference traces (also known as pilot traces). The lateral summation in mixing enhances the event waveform of the pilot traces by averaging out random noise, and averages out the trace-to-trace shifts, or statics, so that their net effect is only a slight broadening of the event waveform. This works well as long as the lateral mixing window is long enough to average the contiguous static shifts to nearly zero, and as long as the average static shift is less than half the wavelength of the event waveform. For large statics, or for those whose average is not near zero, ensemble trace mixing creates waveforms which are broadened, have extra lobes, and may have a bulk shift not representative of the actual underlying event waveform. Also, if the underlying reflection events contain geological structure whose time magnitude is a significant fraction of the event wavelength, the trace-mixed waveform will also be smeared out or contain extra lobes (loop-skipping), making it unsuitable for reference traces.

To remove the smearing effects of structure in the reflections, we have found it useful to apply the trace-mixing along the structure by flattening the reflection events to a picked horizon before mixing. A suitable horizon can usually be picked on a CMP stack of the raw data. The structure can subsequently be restored to the reference wavefield by ‘unflattening’ the mixed trace ensemble. When geological structure is complex enough that deep and shallow reflection events are not relatively parallel, it may be necessary to independently flatten the trace ensemble to more than one horizon and apply trace mixing. The results of trace-mixing along more than one reflection can then be merged to form the reference wavefield (Henley, 2012a).

To reduce the smearing effect of short-wavelength statics on the reference wavefield estimate, we often apply one or more passes of a ‘trim statics’ technique to the raw traces, usually before flattening to a horizon. Trim statics methods are simple algorithms which try to align trace waveforms within a time gate over a lateral window, using correlations of individual traces with the sum of all the traces in the window. This is a ‘brute force’ technique whose only aim is to align waveforms to improve event coherence, and its success depends largely on the width of the time gate used and the S/N of the individual raw traces. Often, ensemble event coherence is only marginally improved by application of trim statics; and sometimes, the coherence actually decreases due to loop skips forced into the events by the procedure. Experience has shown that application of the trim statics

procedure prior to horizon flattening and trace-mixing generally helps raypath interferometry to converge on a solution in one or two iterations; but that the interferometry can still produce a very similar solution without the trim statics operation in the pilot trace estimation, except requiring perhaps 3 or 4 iterations. The more robust the reference wavefield estimate, the more quickly raypath interferometry converges.

As can be seen from the preceding paragraphs, the process of estimating a reference wavefield from a raw trace ensemble is basically that of simplifying the information in the raw ensemble by removing its random noise, random trace shifts, and temporarily, its underlying geological structure. In 2012, Yedlin suggested that Singular Value Decomposition might be a technique that could fruitfully be used to produce similar results, or possibly even better results. This method is actually a family of related techniques based on the idea that decomposing a matrix (representing a wavefield) in a particular way yields components which are distinguished by the increasing amount of detail contained in components of increasing order. In other words, the lowest order components contain the longest wavelength, least detailed parts of the wavefield, and the highest order components contain the most detail, often the random noise. By decomposing a raw trace ensemble matrix into its components, we can construct a new matrix from its lowest order components, and the resulting matrix will be a simpler, more coherent version of the input matrix—a reference wavefield candidate. The nearest implementation of such a method that we found was the 'Eigenvector filter' operation in ProMAX. This operation decomposes the input matrix, presumably a trace ensemble, into its component eigenmatrices, and allows, via a parameter selection, the use of any subset of eigenmatrices to reconstruct the trace ensemble. In our application, we choose only the lowest order eigenmatrices to construct a trace ensemble with little lateral variation and a uniform representation of event waveform.

Trace mixing to create reference wavefield

Raypath interferometry was applied to the RT-filtered, deconvolved Hussar PP data in two passes; first to the source gathers, then to the receiver gathers. After the CMP stack of the resulting gathers, Gabor deconvolution was applied to boost high frequencies, then FX deconvolution to reduce random noise. In this case, the reference wavefield was constructed for each common-raypath gather using simple trace mixing with a mixing length of 201 surface stations for the first pass, 51 stations for the second pass. Each common-raypath gather was flattened to a 1100ms horizon, and trim statics applied, before the trace-mix operation. Figure 7 is the resulting CMP image, which is quite comparable to the conventional CMP stack in Figure 6. The finer details on the 1100ms target horizon appear to be at least equally resolved on this image, if not slightly better, and the shallower reflections are slightly more coherent and prominent.

If we eliminate the trim statics step, but still apply trace mixing along the horizon direction, we find that the initial reference wavefield estimates are less robust, and that the raypath interferometry procedure can still find a good solution, but that three or four passes are required, each with an updated reference wavefield estimate, rather than two. Also, doubling the trace-mixing length for the first two passes improves the performance. Figure 8 displays the result of four passes of raypath interferometry, alternating between the source and receiver gather domains. While the image differs in minor ways from that

in Figure 7, the differences aren't considered significant. The point of this comparison is to show that the trim statics operation has no real affect on the final raypath interferometry solution; it simply speeds up the procedure by improving the initial reference wavefield estimates.

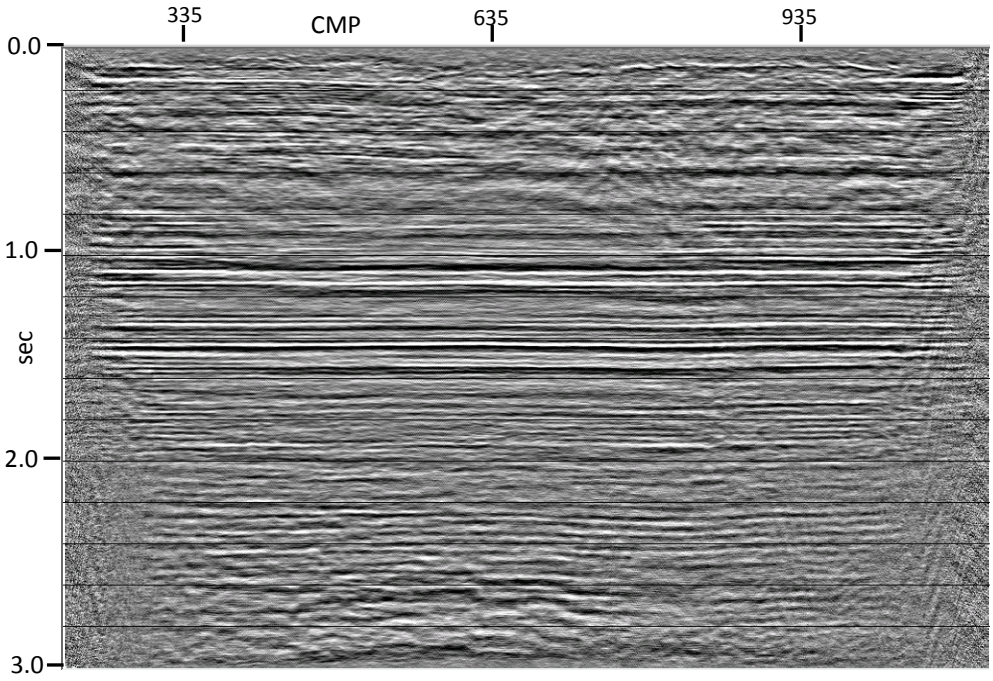

FIG. 7. CMP stack of Hussar PP dynamite data using single NMO function and raypath interferometry. Trace mixing used for reference wavefield estimation. Trim statics used to assist trace alignment prior to mixing--two passes of interferometry used.

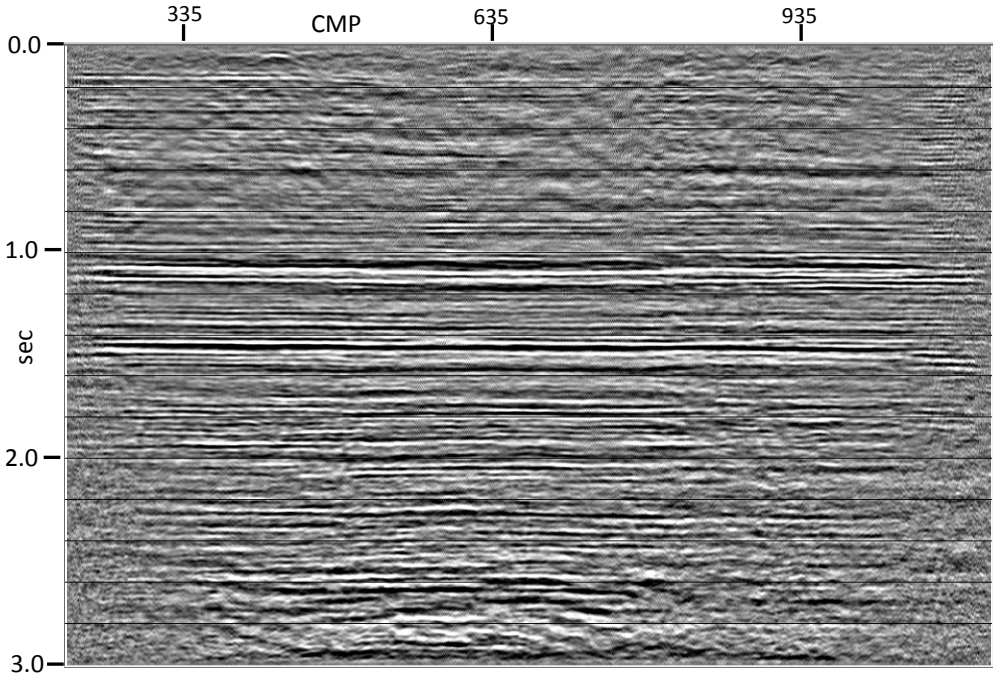

FIG. 8. CMP stack of Hussar PP dynamite data using single NMO function and raypath interferometry. Trace mixing used for reference wavefield estimation. No trim statics applied—four passes of interferometry used.

Eigenvector filtering to create reference wavefield

The eigenvector filter operation in ProMAX decomposes a matrix corresponding to an ensemble of seismic traces into the weighted sum of a series of separable matrices, or 'eigenimages', each corresponding, in succession, to information of higher wavenumber. By discarding the higher rank matrices before summation to reconstitute the original matrix, a kind of smoothing is imposed on the original matrix. The effective smoothing length for this operation is controlled by a parameter which specifies what percent of the range of eigenimages (eigenmatrices) from the original decomposition will be included in the reconstruction. Experimentation showed that restricting this parameter to less than 1% provided the best smooth reference wavefield estimates for the first pass of raypath interferometry. Figure 9 shows the result of one pass of raypath interferometry using only the lowest rank 0.5% of the common-raypath gather eigenimages to form the reference wavefield. The result is comparable to, or even slightly better than the one-pass result shown in Figure 10, where trace mixing was used to create the reference wavefield. If we add a second pass of raypath interferometry using the lowest 2.0% of the eigenimages of the common-raypath gathers (to allow a bit more detail into the reference wavefield estimates), the result is shown in Figure 11, which should be compared to Figure 7.

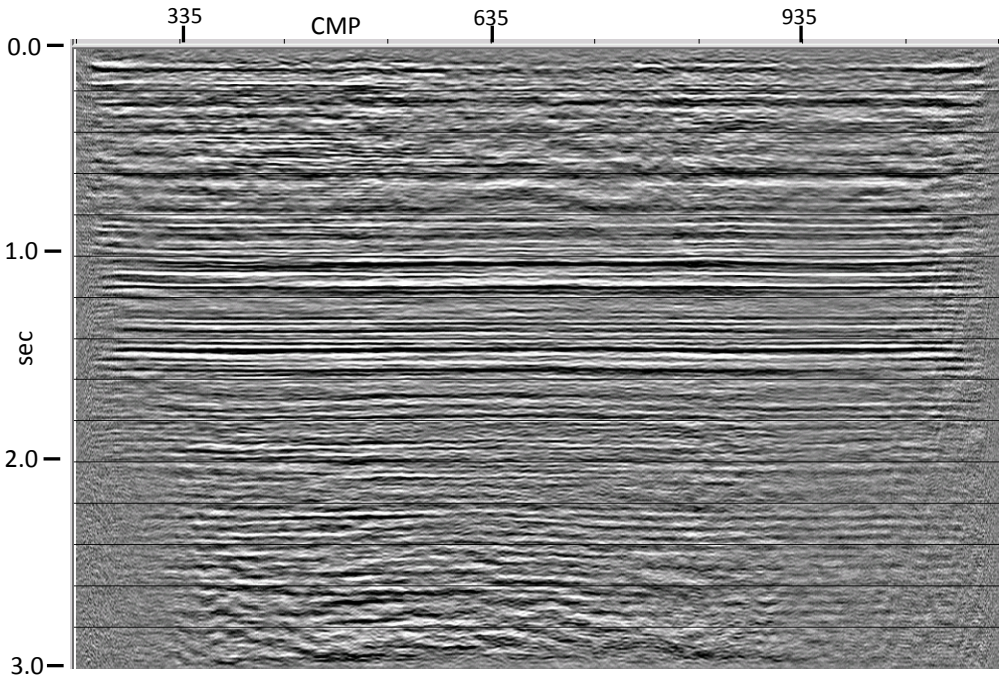

FIG. 9. One pass of raypath interferometry applied to Hussar PP dynamite data using single NMO function and 0.5% of the lowest rank eigenimages for reference wavefield estimates.

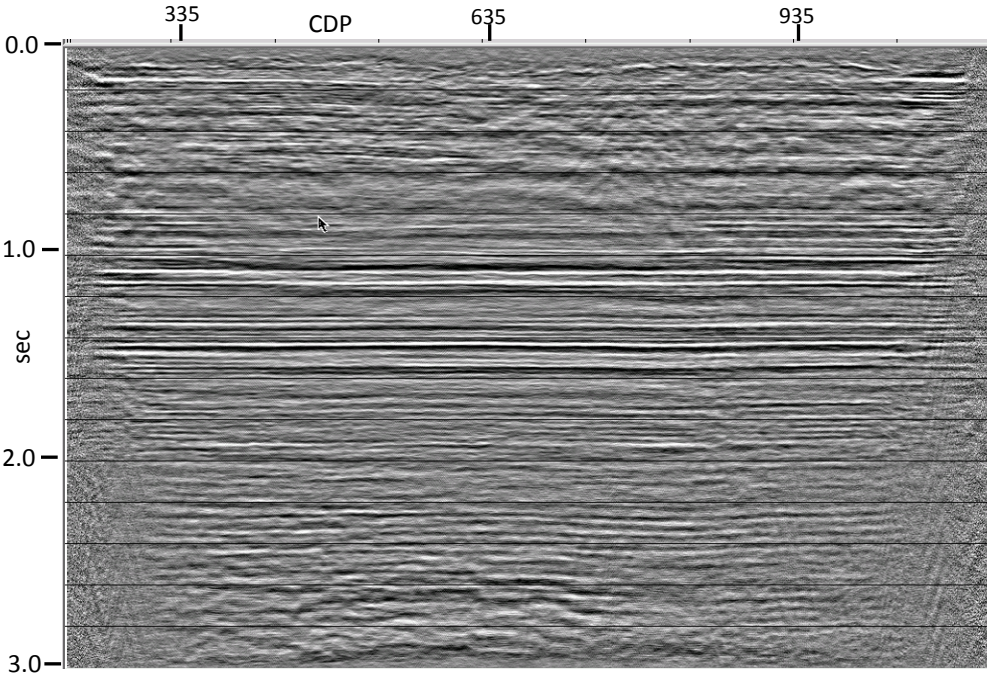

FIG. 10. One pass of raypath interferometry applied to Hussar PP dynamite data using single NMO function and trace mixing to estimate reference wavefield.

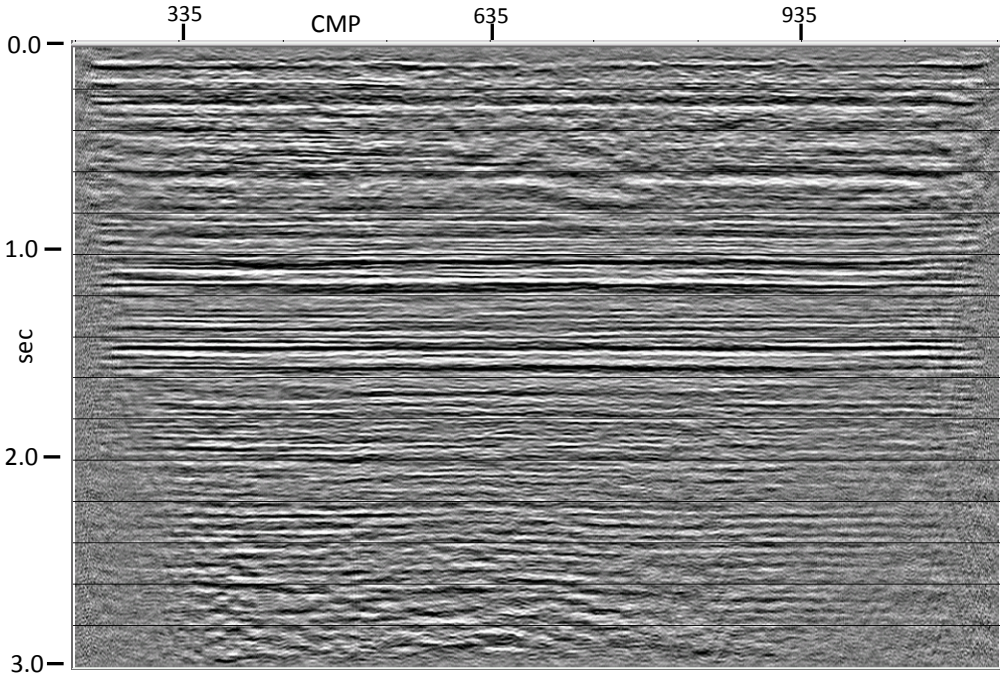

FIG. 11. Two passes of raypath interferometry applied to Hussar PP dynamite data using single NMO function and low-rank eigenimage reconstruction for wavefield estimation—low order rank limits 0.5% for first pass, 2.0% for second pass. Compare with Figure 7.

In our testing, we found that the choice of the rank-limiting parameter was not very sensitive, as long as the parameter was sufficiently small. When this parameter exceeds 10%, the common-raypath reference wavefield gathers retain sufficient lateral detail from the initial raw gathers to degrade the performance of the interferometry, a similar effect to reducing the mixing length too much for trace-mixing. Interestingly, applying trim statics before eigenvector filtering does not seem to improve the wavefield estimate much, since the lateral discontinuities in the wavefield caused by statics in the raw data are contained mostly in the higher rank eigenimage components. This means that the wavefield estimate reconstructed from the selected low rank components will have low amplitude gaps corresponding to groups of input traces with significant statics. Such gaps can be bridged by applying median mixing to the eigenvector filter results.

On the other hand, while trace mixing can sometimes produce usable results on gathers which haven't been flattened to a horizon (as long as the structure is very mild), eigenvector filtering tends to fail by putting lateral steps in the wavefield in place of a smooth structure. To illustrate some of these differences in reference wavefield estimation, Figure 12 displays a raw common-raypath gather from the Hussar data set, corresponding to a raypath parameter of -500m/s. Due to the noise, the underlying reflections are obscured on much of this gather. Applying horizon flattening leads to the image in Figure 13, where the reflections are more apparent, due to being better aligned horizontally. When we apply 201-station trace mixing, the reference wavefield estimate in Figure 14 appears; and when we additionally apply trim statics before the trace mixing, the improved estimate in Figure 15 appears. To compare, the wavefield estimate constructed using 0.5% of the lowest rank eigenimages is displayed in Figure 16, and the

same estimate filled in laterally by 101-station median mixing is shown in Figure 17. If no horizon flattening is applied first, the eigenvector filter result prior to median mixing is shown in Figure 18; but the application of the median mix gives the same result shown in Figure 17.

Based on the results shown above, we would conclude that SVD or Eigenvector filtering, as implemented in ProMAX is a viable alternative to trace-mixing in the construction of a reference wavefield for the raypath interferometry technique. For either technique, good results in most cases require flattening the input common-raypath gathers to a horizon, hence guiding the mixing or the eigenvector filtering along the reflection structure. In the case of trace mixing, trim statics applied prior to the mixing operation significantly improves the result, leading to faster convergence of the interferometry result; but the operation is not mandatory unless statics are so large that the mixed results exhibit significant loop skipping. For eigenvector filtering, on the other hand, an operation like median mixing seems to be required to bridge the discontinuities evident in the filtered results. Trim statics appears to provide no real benefit, since the median-mix seems to be necessary, regardless. Intuitively, we expect that eigenvector filtering will work best on high S/N data with relatively small statics, while trace-mixing will perform best on data with low S/N and or very large statics, but in the latter case may require trim statics to speed the convergence.

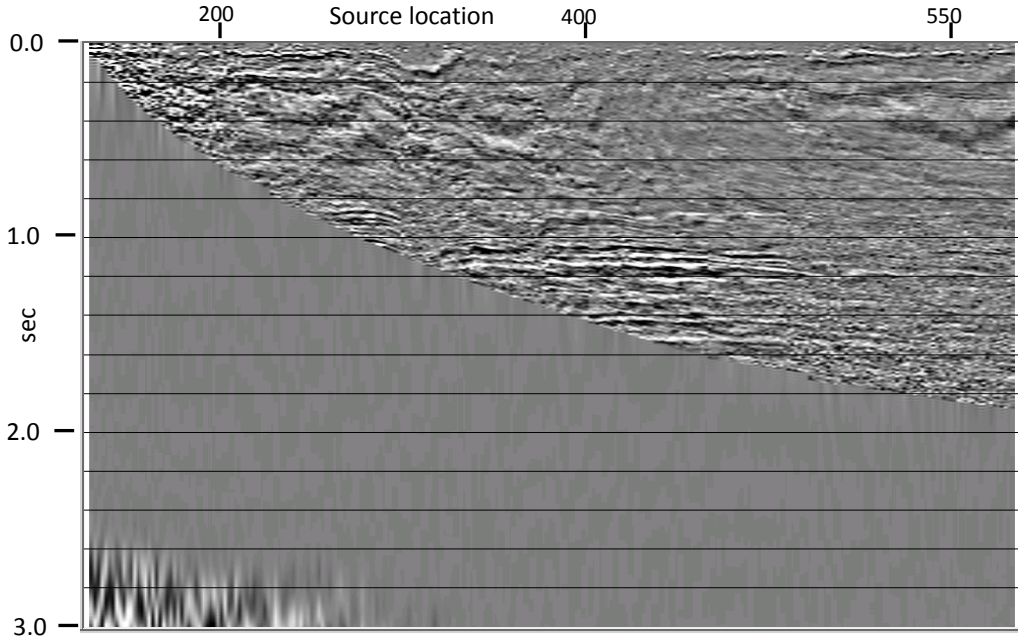

FIG. 12. Raw common-raypath gather for raypath parameter = -500m/s. Reflections are partially obscured by noise and not well-aligned.

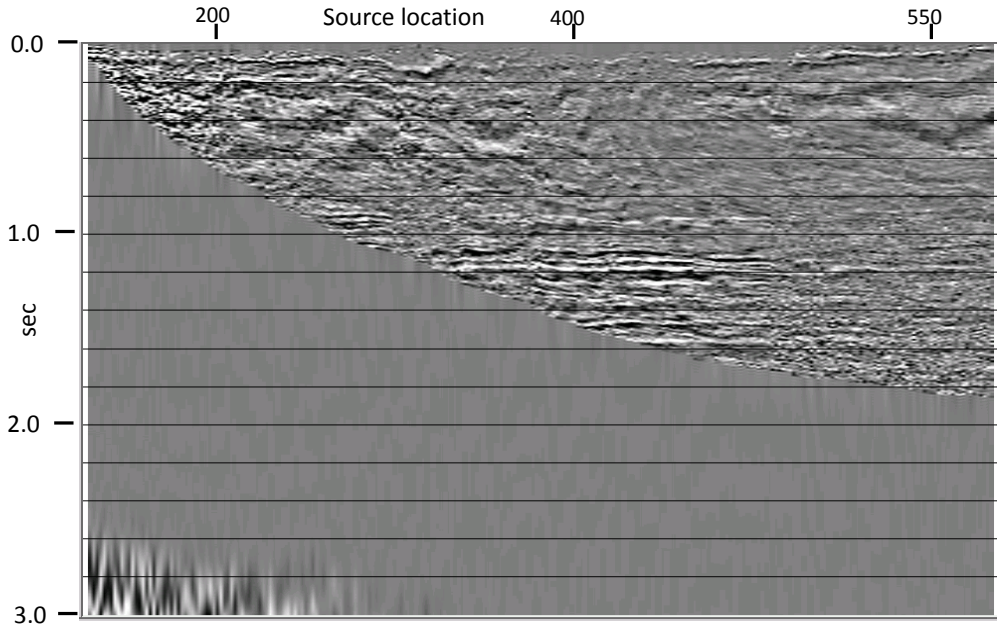

FIG. 13. Raw common-raypath gather for raypath parameter = -500m/s. Horizon flattening has been applied, and event alignment is more apparent.

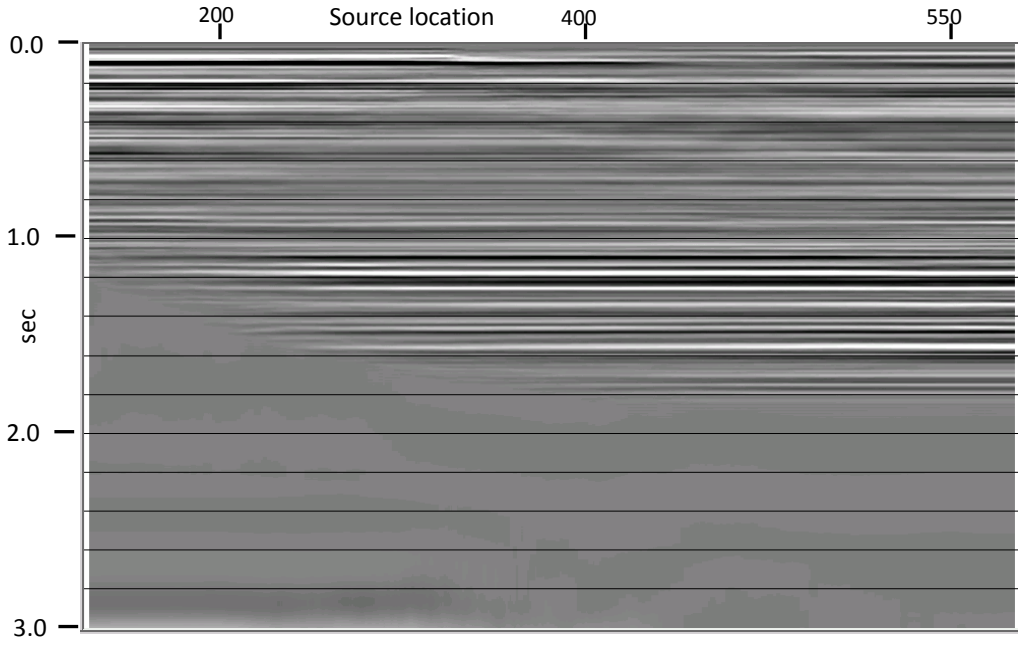

FIG. 14. Wavefield estimate for raypath parameter = -500m/s. 201 trace mixing operator used for estimation.

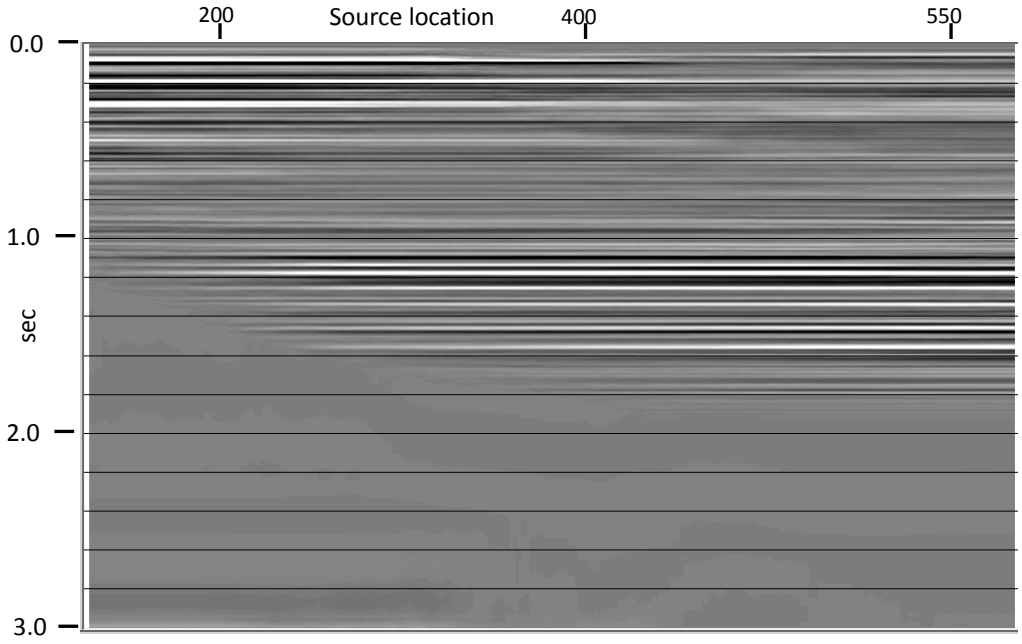

FIG. 15. Wavefield estimate for raypath parameter = -500m/s. Close comparison of this figure with Figure 14 shows that trim statics (applied before the trace mixing) used in this estimate improves the continuity of the estimate, especially for shallow events.

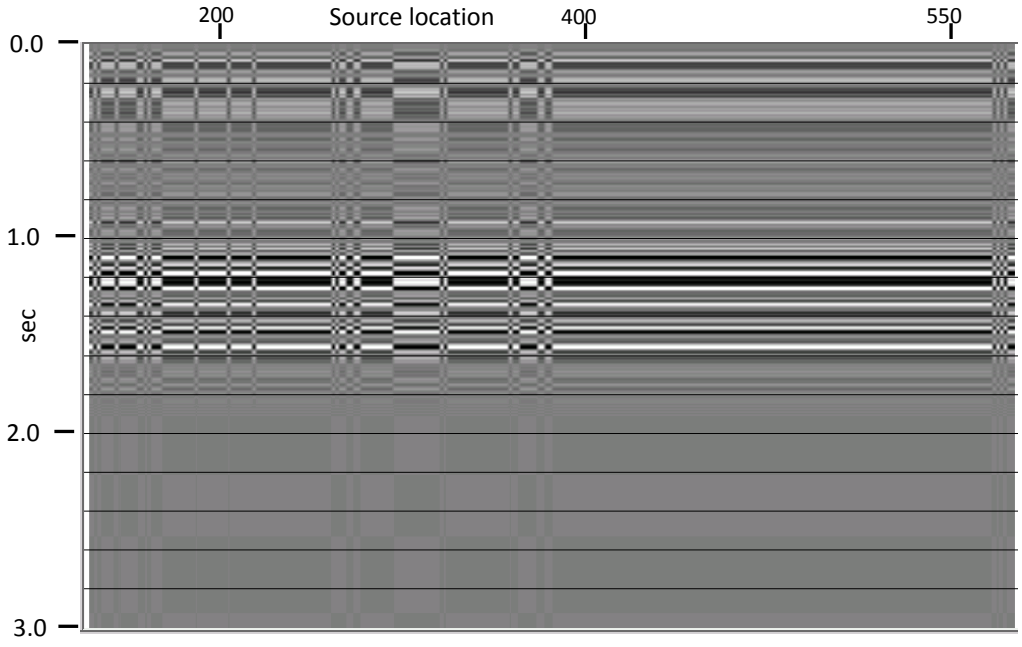

FIG. 16. Wavefield estimate for raypath parameter = -500m/s. Lowest 0.5% rank of eigenimages used for estimate. Discontinuities (basically polarity reversals) are characteristic of this method.

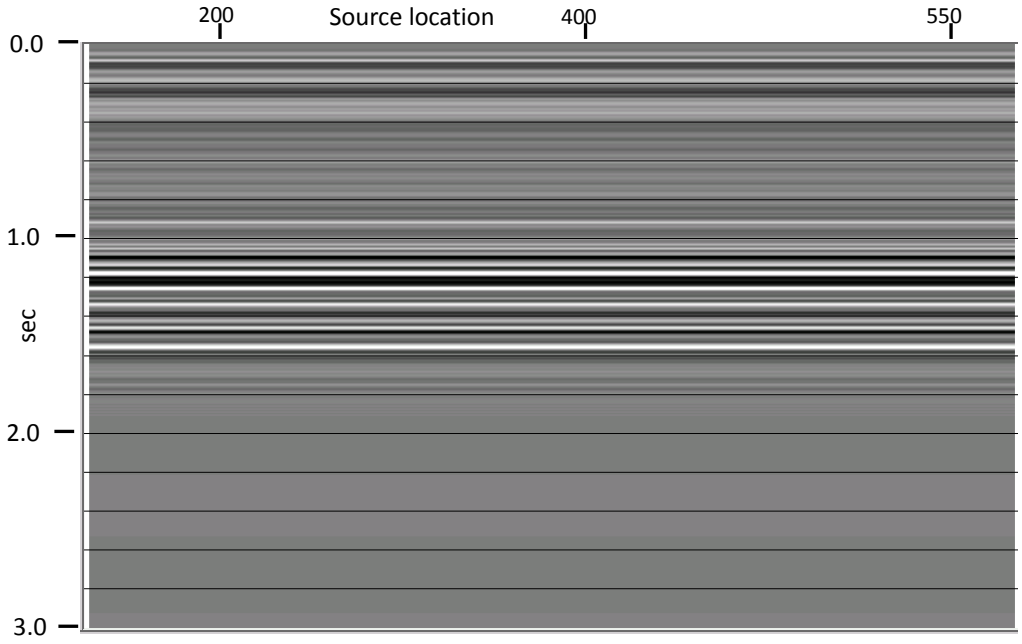

FIG. 17. Wavefield estimate for raypath parameter = -500m/s. Lowest 0.5% rank of eigenimages used for estimate. Median mixing (101 traces) has been used to fix discontinuities and make this estimate usable.

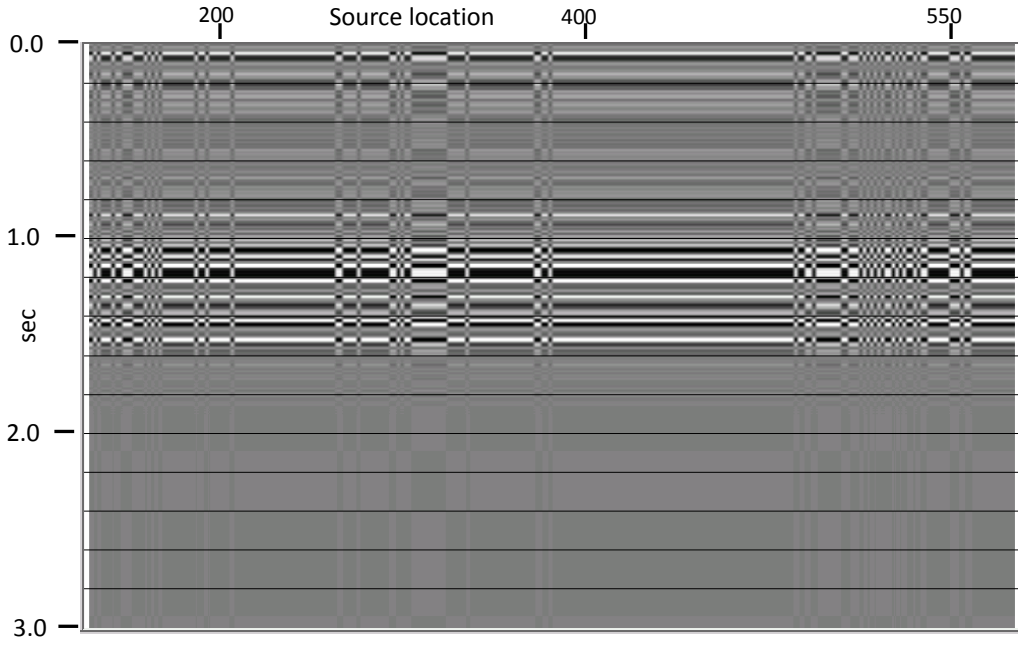

FIG. 18. Wavefield estimate for raypath parameter = -500m/s. Lowest 0.5% rank of eigenimages used for estimate. When no horizon flattening is applied prior to eigenimage estimation, even more discontinuities appear than in Figure 16. Nevertheless, the same 101 trace median mixing operator applied to this estimate gives the result shown in Figure 17.

Transforming to the common-raypath domain

In all previous work, we have used the conventional radial trace transform to map raw seismic trace gathers into a new domain where a 'raypath parameter' is one coordinate of the data amplitude values. The RT transform uses linear trajectories in the X-T domain to extract samples to map into the new domain, and this corresponds physically to straight raypaths in the earth, regardless of reflection boundaries and the subsequent refraction of actual raypaths in the earth. While this is a good first-order approximation, it makes sense to attempt to conform the RT sampling trajectories more nearly to the actual raypaths in order to better capture seismic amplitudes which are properly associated with those raypaths. Fortunately, there is a closely related transform, the Snell Transform (Claerbout, 1975, 1985; Ottolini, 1982), which attempts to do just that. In the Snell Transform, the sampling trajectories in the X-T domain each have an initial raypath parameter (apparent velocity), which is associated with that particular raypath, just like in the RT Transform. However, in the Snell Transform, each trajectory is bent from its initial value as its depth increases, to conform to Snell's Law. We have currently implemented two ways to perform this bending: extracting interval velocities from a supplied NMO velocity function, smoothing them, and computing a refractive index function; and simply choosing a single gradient which determines a monotonic refractive index increase with depth.

While the first method seems most intuitively correct, it often requires significant experimentation to create an acceptably smooth set of sampling trajectories. NMO velocity functions which reflect relatively large changes in rock properties at reflection boundaries often lead to unrealistic interval velocities, which, even smoothed, can lead to unappealing Snell Transforms, with gaps or holes in the data for certain ranges of raypath parameters. Transforms computed from smoothly increasing refractive index profiles, on the other hand, have no such gaps and are more 'esthetically pleasing', even though they may not reflect the actual raypaths as realistically. We have been able to get good results with either type of Snell Transform, so evidently, esthetic appeal isn't a necessary criterion for judgement.

The Hussar converted wave data set

In what follows, we will use not only the Hussar PP dynamite data set, but also the accompanying PS (radial accelerometer component) data, since the shear-wave statics for that data set appear to be nonstationary. Accordingly, we show first a 'brute' (no statics) CCP (common conversion point) stack of those data in Figure 19, where only one NMO function has been used for the entire line. This image reveals that not only are the coherent reflection events disrupted by apparent unresolved statics at several locations along the line, but that the missing statics, as well as residual NMO corrections would be required to make the PS events flat. That they should be flat (no structure) is clear from the PP images shown previously of the same geological section. A further diagnostic image for these data is the common-receiver stack shown in Figure 20, also using the single NMO function. The large receiver statics required to make the events coherent are readily apparent here, as is the fact that larger statics appear to be needed for shallow events than for deeper ones at the same CCP locations (nonstationary statics). The false

long-wavelength structure on the reflections is also quite clear on this image, amounting to well over 100ms from one end of the line to the other.

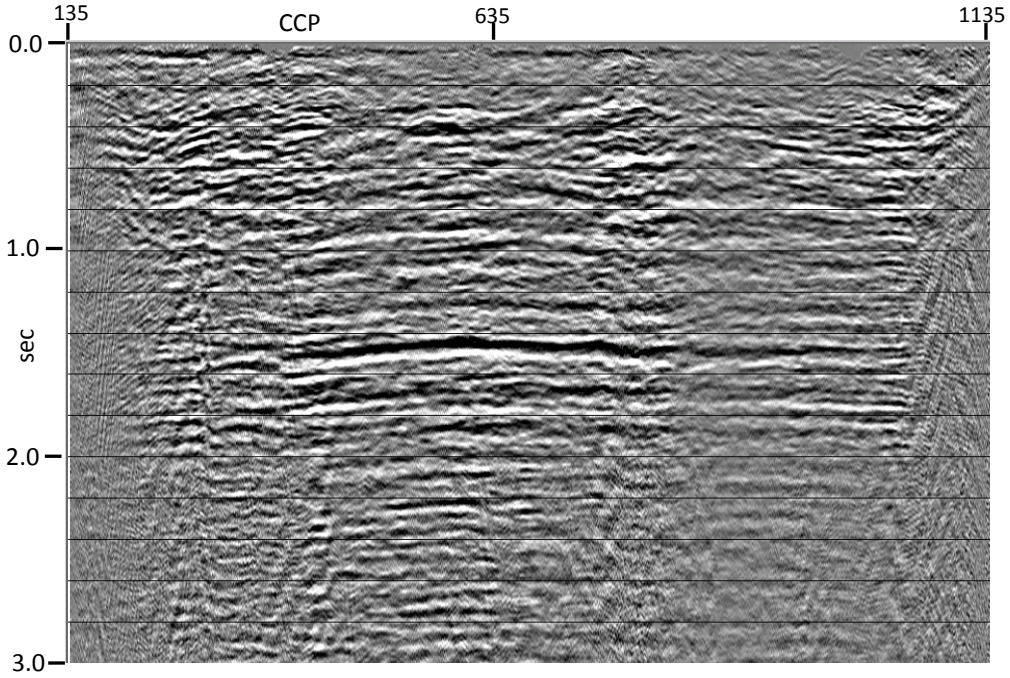

FIG. 19. Brute CCP stack of PS dynamite data from Hussar. Single NMO function used, and no statics have been applied.

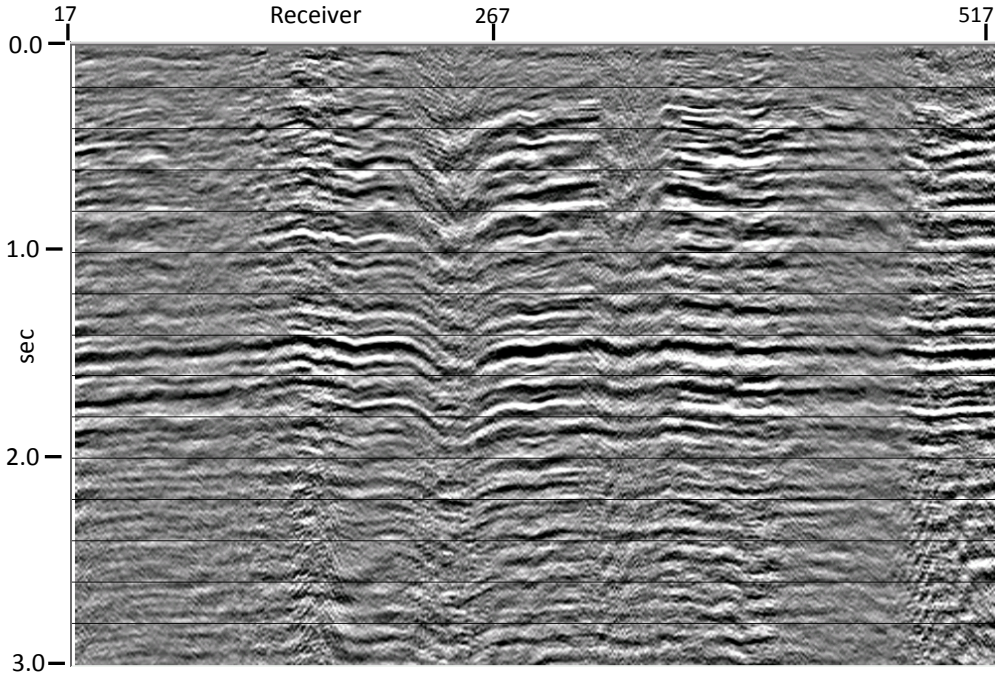

FIG. 20. Common-receiver stack for Hussar PS dynamite data. Non-stationary statics and false structure are both evident on this display.

In fact, conventional NMO analysis and residual statics techniques can be made to provide reasonable results for these data, as shown in Figure 21. It should be noted, however, that events above 1000ms are low in amplitude and exhibit zones of incoherence in the vicinity of known large statics as seen in Figure 20. Since the events in this image are flat, as they should be, it is evident that the combination of conventional statics methods and residual NMO analysis and correction has accommodated, at least partially, the apparent non-stationarity of the receiver statics.

Figure 22 displays the CCP image obtained using raypath interferometry on these data. Since the largest statics are the receiver statics, the data were sorted to receiver gathers, and the first pass of interferometry was made in that domain. The interferometry process whitens the data somewhat, and the image isn't completely comparable to Figure 21; but some of the more interesting differences are in the increased amplitude and coherence of shallow events on the interferometry results. Interestingly, events deeper than 2000ms are not as strong or coherent as on the conventionally processed image. Differences in the NMO functions used to stack the two images also lead to some reflection time discrepancies between comparable events; a better choice of NMO function for the interferometry results would reduce these discrepancies. To show that the raypath interferometry process has corrected both the apparent nonstationary statics and the false structure while still using only a single NMO function, we show the common-receiver stack in Figure 23, to compare with Figure 20.

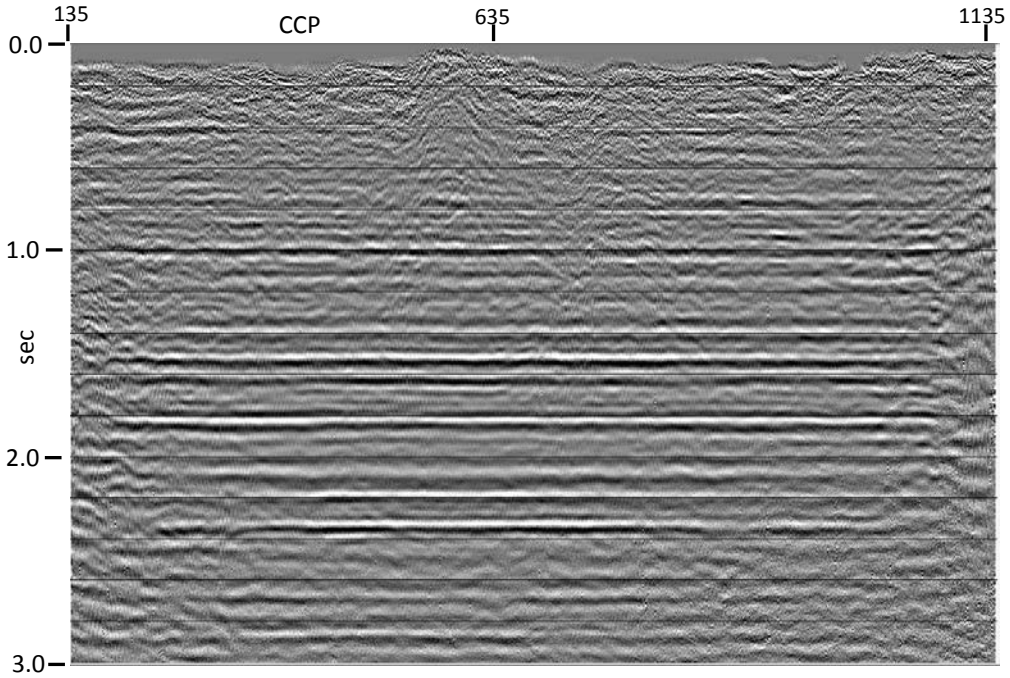

FIG. 21. CCP stack of Hussar PS dynamite data after NMO analysis and conventional statics.

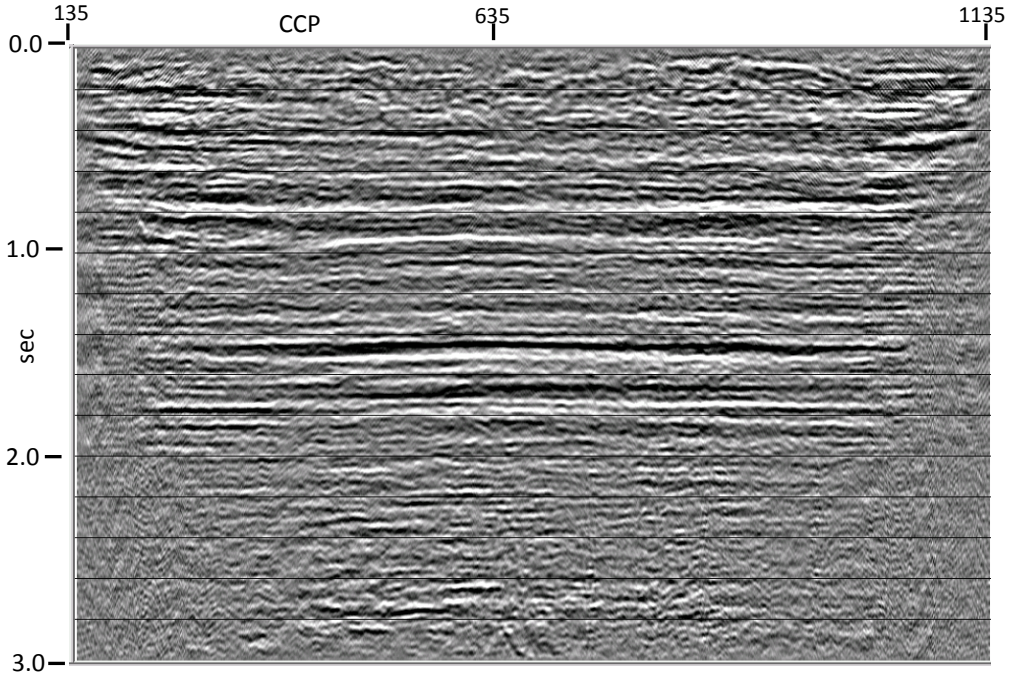

FIG. 22. CCP stack of Hussar PS dynamite data after raypath interferometry using a single NMO function. Shallow events in this image are stronger and more coherent than the same events in Figure 21.

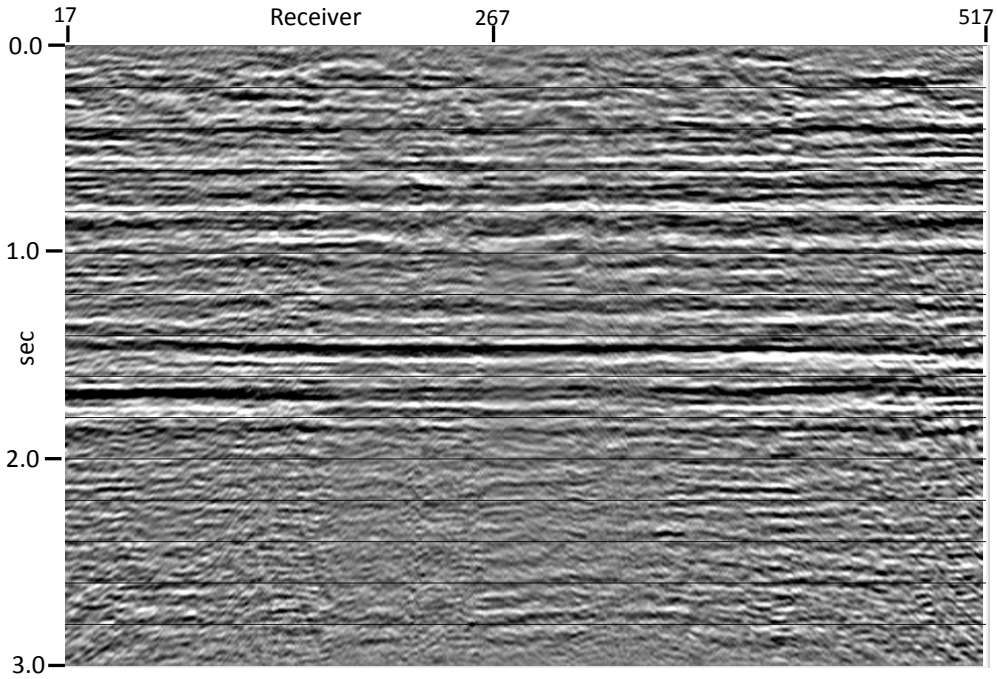

FIG. 23. Common-receiver stack of Hussar PS dynamite data after raypath interferometry using a single NMO function. Nonstationary statics and false structure shown in Figure 20 have been corrected without forcing the corrections into residual NMO.

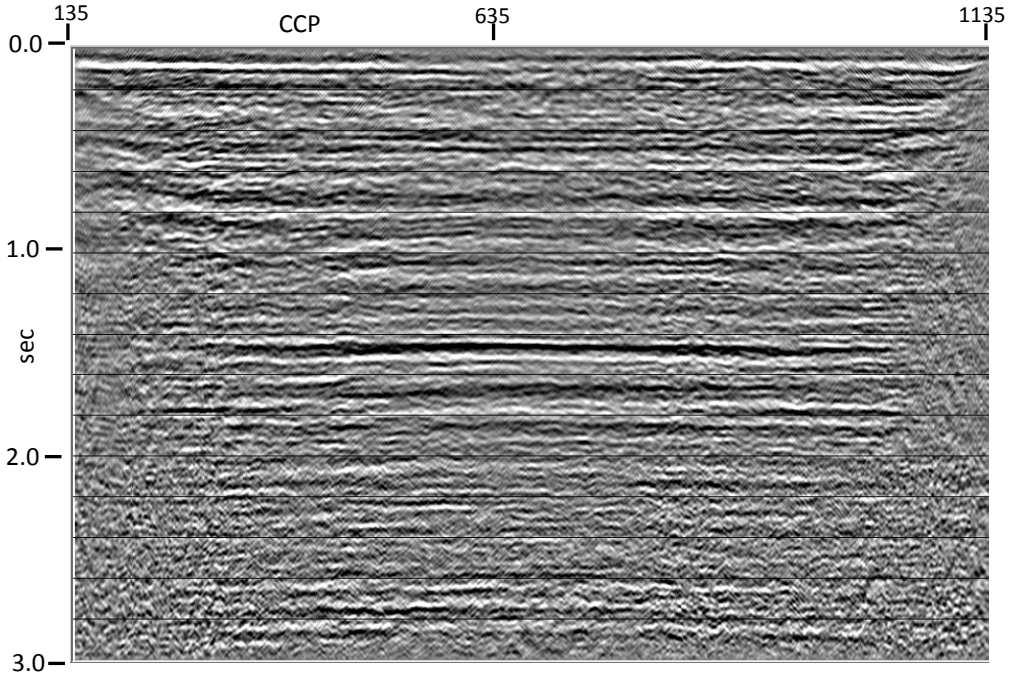

FIG. 24. CCP stack of Hussar PS dynamite data after raypath interferometry using a single NMO function. For this run, the trim statics step was eliminated from the reference wavefield estimation process; yet the image still converged in just two passes of interferometry.

In another test of the robustness of the reference wavefield estimation process, we removed the trim statics step from the wavefield estimation process, allowing the horizon-flattening and trace-mixing processes to accomplish the whole task. As can be seen in the CCP stack in Figure 24, even in the presence of these large receiver statics, the wavefield estimation process works well enough to lead to convergence of the solution, this time in only two passes. The apparently continuous events above about 200ms on this image should be disregarded, however, since it is likely that they are just fortuitously stacked unmuted direct arrivals at small offsets (we never apply muting to raw trace gathers, relying on radial trace filtering to attenuate arrivals instead).

Snell Ray Transform using smoothed interval velocities

To introduce the Snell Ray Transform, we first display a conventional RT transform created with linear trajectories, in Figure 25. The transform corresponds to shot number 257 of the Hussar PP data set; and the major reflections are readily visible. To generate an interval-velocity-guided Snell Ray Transform, we computed interval velocities, using the Dix formula, from the NMO velocity function, then applied 51-point smoothing to the interval velocities to soften the large velocity contrasts. The smoothed interval velocity function was then converted to incremental refractive index values and used to trace each sampling trajectory for the Snell Ray Transform for shot 257, shown in Figure 26. The influence of the interval velocity function can be seen at the edges of the transform, as well as in the near-vertical noise events near the centre, where ‘kinks’ can be observed. While unsightly, these manifestations of the velocity function do not affect the operation of the interferometry procedure, since even ‘weird’ transforms like that in Figure 26 can be inverted exactly. More important are the results we can obtain by using this transform

to represent potential raypaths compared to the more 'approximate' standard RT transform. Note on both figures a curved, dashed trajectory, which traces one of the original XT-domain traces from this shot gather. It is interesting to see that the statics variations visible in the vicinity of these trajectories on each figure seem to align well with the trajectories. This confirms that the statics are indeed surface-consistent for these data. The vertical red trajectories shown on both figures, on the other hand, show how statics anomalies on various reflections align in the common raypath direction on both displays. In Figure 25, we see that the anomalies on shallower reflections do not align well with those on deeper reflections (white circle and arrows), indicating that the linear RT construction does not properly capture the static anomaly attributable to a single raypath on all reflections. In this case, each 'common-raypath' trace will lead to interferometric solutions most strongly influenced by the statics anomalies on the strongest reflections on these traces. In this case, a particular static anomaly on a shallow reflection will appear on a different common-raypath trace than the same anomaly on a deeper reflection. This means that the statics solutions for each set of common-raypath gathers will be very similar. In Figure 26, however, because the distorted XT trace trajectory (yellow) more nearly aligns locally with the raypath trajectory (red) we see that deep and shallow statics anomalies are better aligned (white circle and arrows), thus leading to interferometric solutions that are more nearly 'common-raypath' solutions.

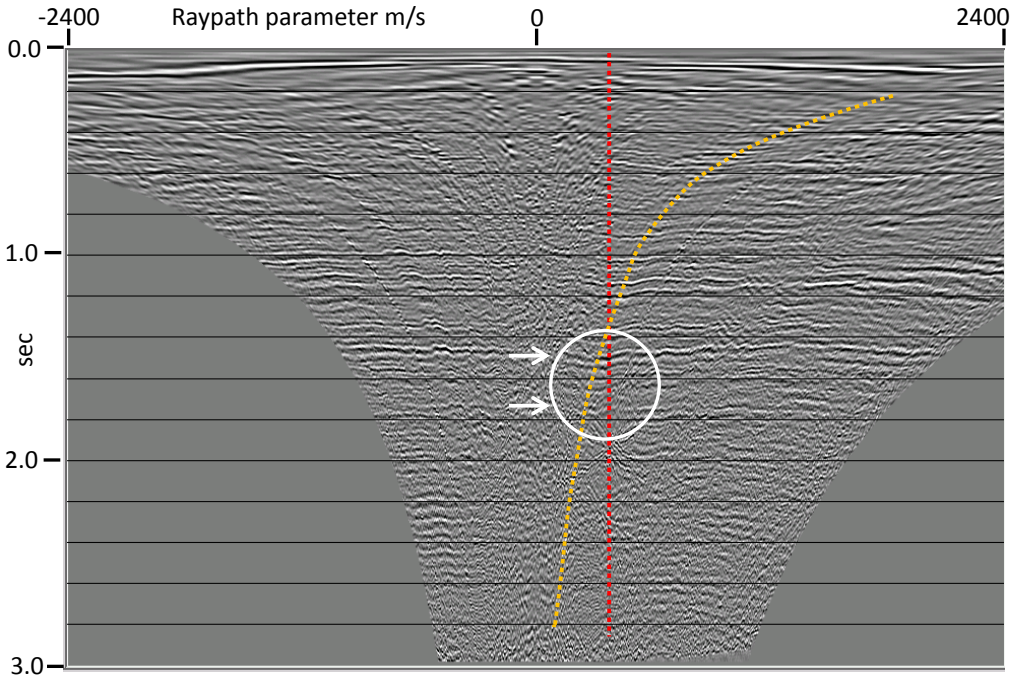

FIG. 25. Conventional RT Transform of source gather 257 of the Hussar PP data set. Yellow trajectory follows an XT trace, while red trajectory shows the common-raypath direction.

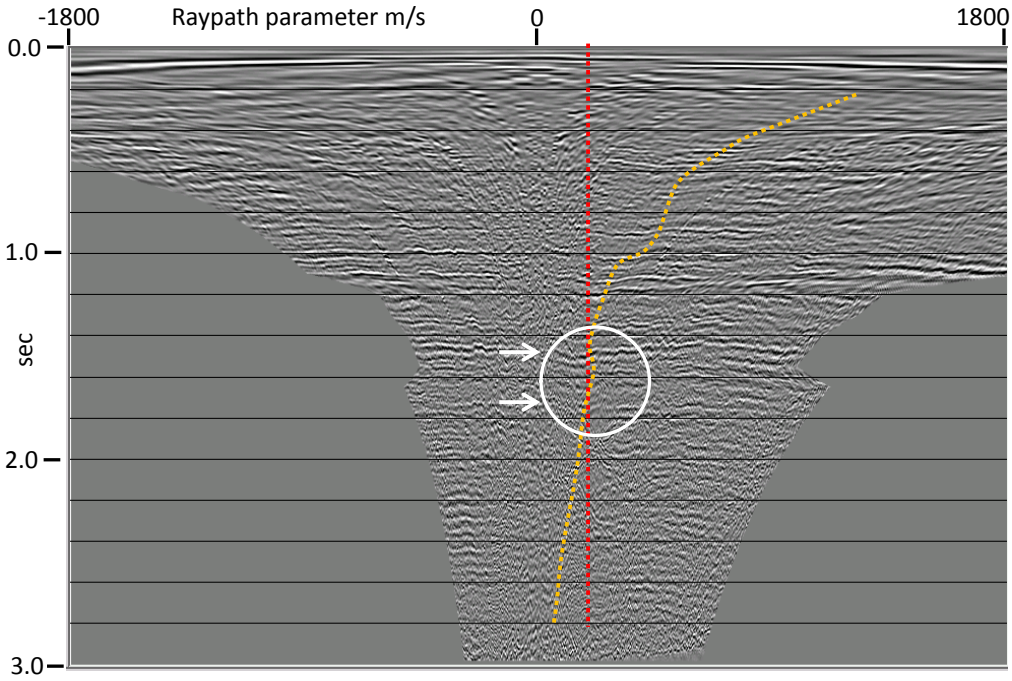

FIG . 26. Snell Ray Transform of source gather 257 of the Hussar PP data set. Yellow trajectory follows an XT trace, while red trajectory shows the common-raypath direction.

Figure 27 shows the CMP image of the Hussar PP data set after two passes of raypath interferometry using the velocity function to create a more 'realistic' Snell Ray Transform. For ease of comparison, we reproduce Figure 7, the CMP stack image using Raypath interferometry using the conventional RT Transform, as Figure 28. Comparing Figures 27 and 28, we see that the prominent reflection complex at 1100ms is quite comparable between the two images, with similar continuity and detail. If anything, there seems to be more detail at that level in the Snell Ray results. Furthermore, the shallow portion of the image shows significantly more detail and continuity in all the layers (disregarding the event at 100ms, which is likely a direct arrival remnant). Events below about 1600ms, on the other hand, appear more continuous in Figure 28, using the conventional RT transform. These differences in the images are likely a consequence of how well the statics variations in the various events align within the common-raypath domain. The primary difference between the RT transform and Snell Ray transform as applied within raypath interferometry is to alter the particular alignment of statics features exhibited on the individual events. This, in turn, alters the statics solutions derived and applied interferometrically to the individual common-raypath gathers.

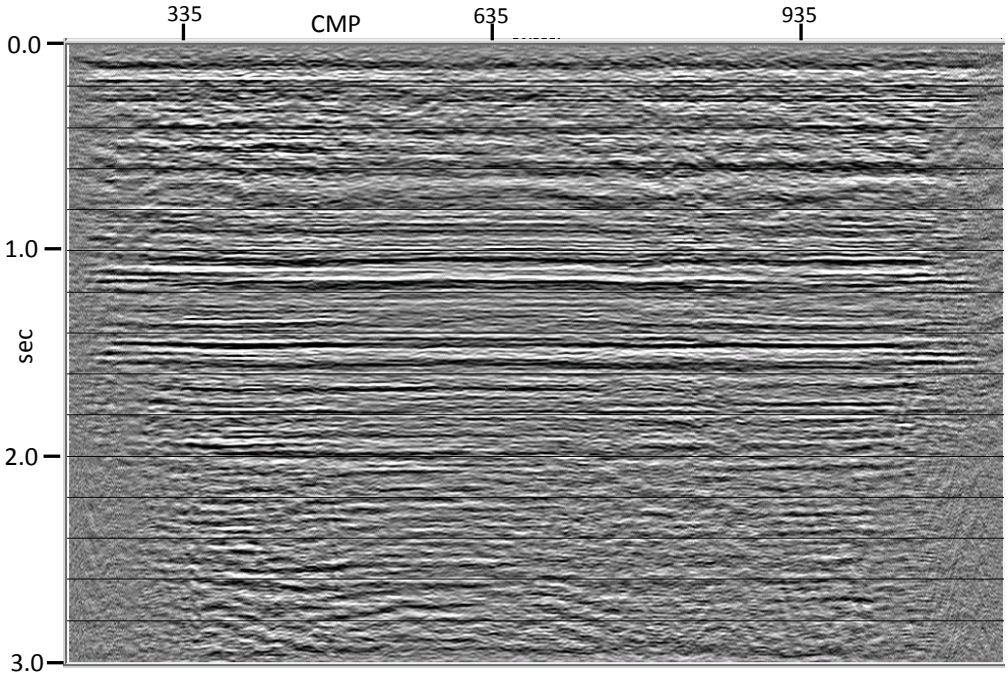

FIG. 27. CMP stack of Hussar PP data after 2-pass raypath interferometry using Snell Ray Transform with 51pt interval velocity smoothing.

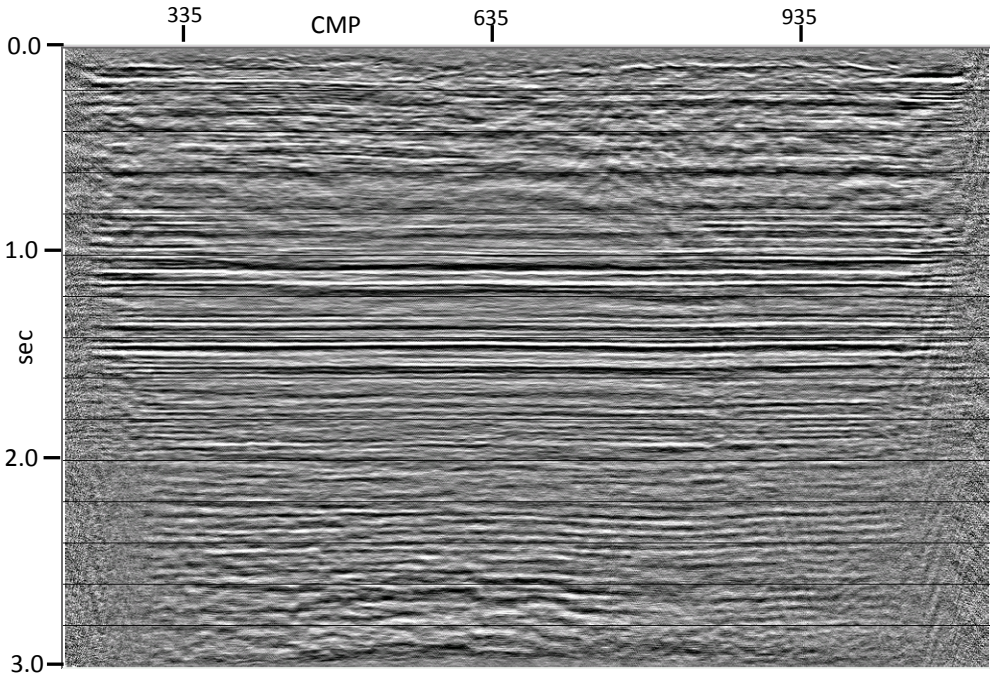

FIG. 28. CMP stack of Hussar PP data after 2-pass raypath interferometry using conventional RT Transform. This figure is the same as Figure 7.

Snell Ray Transform using linear refractive index increase

Figure 29 displays the Snell Ray transform corresponding to shot 257 where the Snell trajectories are created by imposing a simple linear increase on refractive index with travel time. Because this method produces smoothly curving trajectories, the transform has none of the kinks or irregularities sometimes displayed by Snell Rays constructed using interval velocities. The statics irregularities along the common-ray trajectory on Figure 29 show an alignment (white circle and arrows) similar to those in Figure 26 for the velocity-directed Snell Ray Transform. Hence, it is no surprise to find that the CMP stack of the Hussar PP line using the linear refractive index increase version of the Snell Ray Transform, in Figure 30, appears quite similar to that in Figure 27, including increased detail and coherence of the shallow events relative to the linear RT transform result in Figure 28.

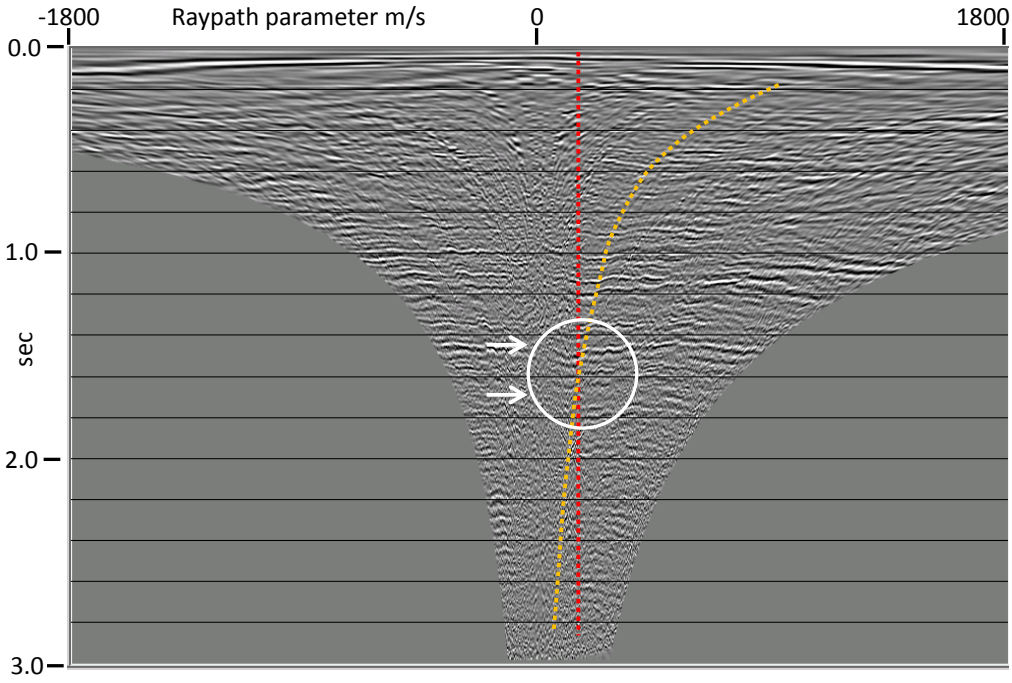

FIG. 29. Snell Ray Transform of source gather 257 of the Hussar PP data set. Yellow trajectory follows an XT trace, while red trajectory indicates the common-raypath direction.

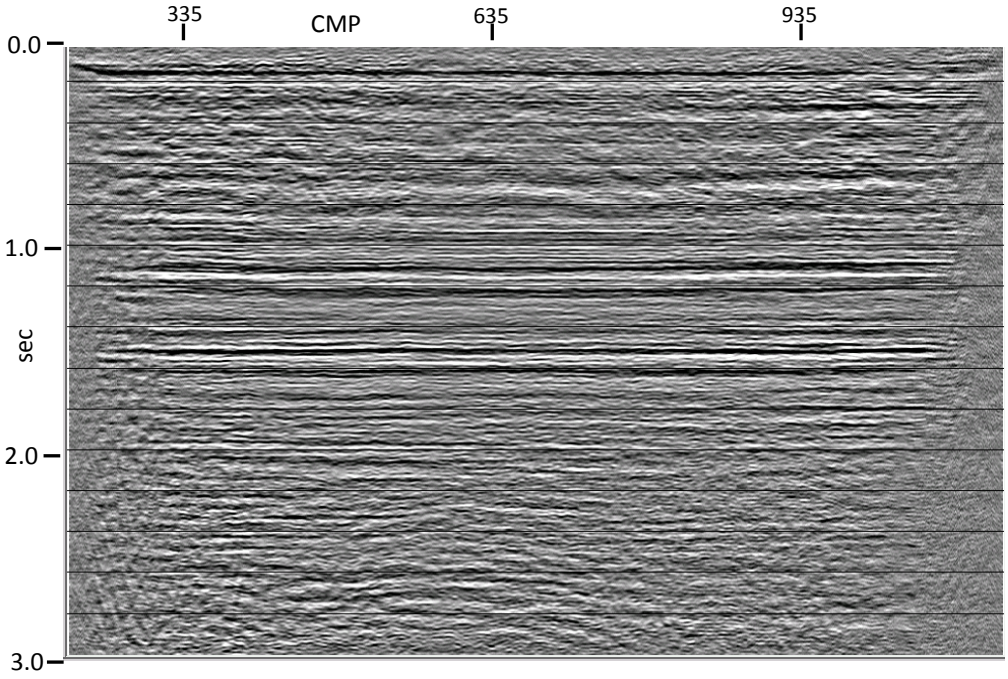

FIG. 30. CMP stack of Hussar PP data after 2-pass raypath interferometry using Snell Ray Transform with smoothly increasing velocity. Compare with Figure 27.

Figure 31 is a repeat of Figure 22, for ease of comparison with Figure 32, which is the CCP stack of the Hussar PS data after raypath interferometry using the Snell Ray transform with a linear refractive index increase. In this comparison, we see improved lateral coherence at all event levels, but a slight decrease in event amplitudes as well as an increase in random noise. The events in Figure 32 are also flatter than those in Figure 31, which is a desirable result.

As a cautionary note, we add Figure 33, which shows the CCP stack image after interferometry using the Snell Ray Transform, but with a much larger refractive index incremental increase. A mistake in processing caused the RT Transform to be used to invert the Snell Ray Transform prior to the CCP stack. Clearly, the highly curved sample trajectories in the Snell Ray Transform have performed a kind of “migration”; the result is an image whose events have actually been shifted to times 200ms shallower than their actual position.

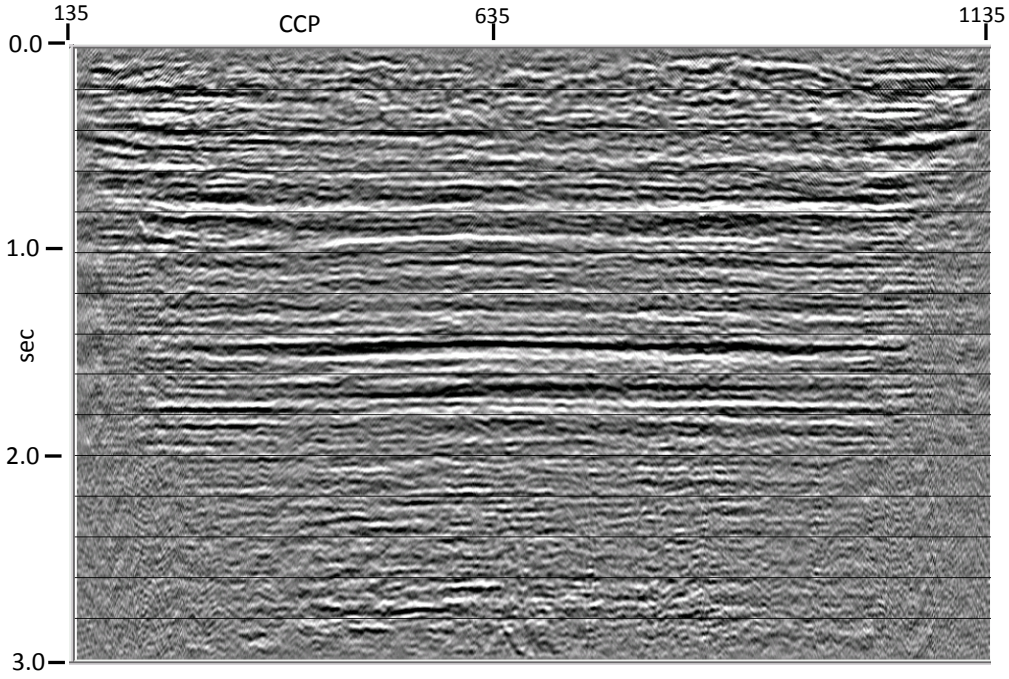

FIG. 31. CCP stack of Hussar PS data after 2-pass raypath interferometry using conventional RT Transform. This figure is the same as Figure 22.

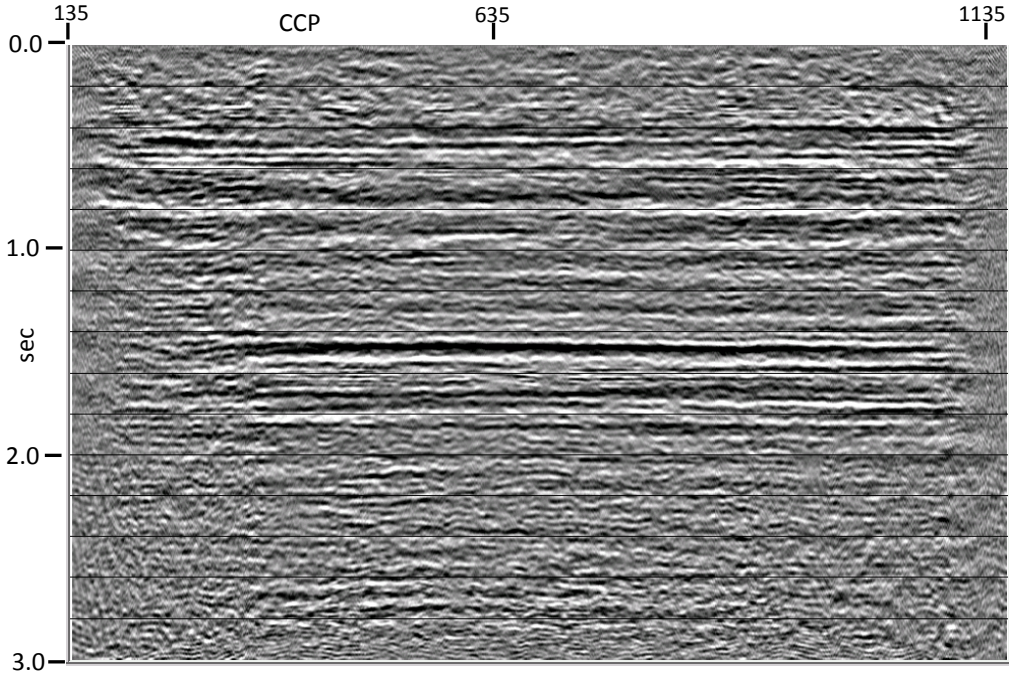

FIG. 32, CCP stack of Hussar PS data after 2-pass raypath interferometry using Snell Ray Transform with smoothly increasing velocity.

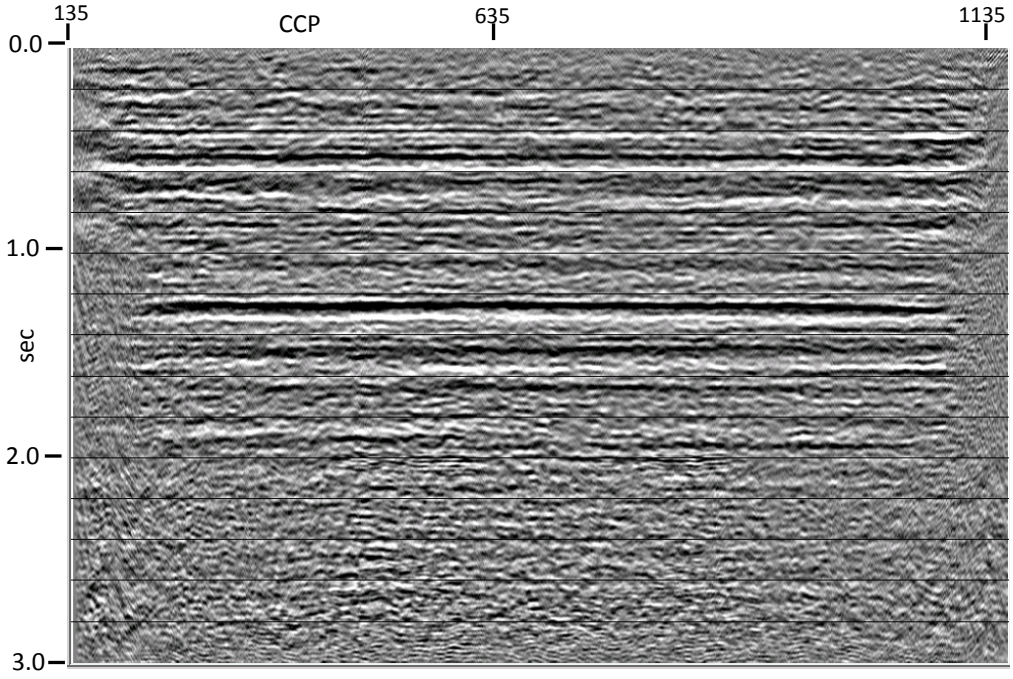

FIG. 33. CCP stack of Hussar PS data set after 2-pass raypath interferometry using the Snell Ray Transform with linear velocity increase. In this case, the velocity increase is too large, resulting in imaged events being shifted to times which are 200ms too shallow.

Figures 34 and 35, respectively, show the RT Transform and Snell Ray Transform of shot 361. The red corridors on each figure show the respective vertical alignment of event variations that are thus considered to be on 'common raypaths'. The large variations shown in three events at different times appear to align better in Figure 35 than in 34, thus verifying that the Snell Ray Transform appears to conform more closely to our common-raypath constraint, thus explaining its slightly better performance for CCP imaging. It is interesting to note, as well, that the statics anomalies shown in these figures align much better in the vertical (common-raypath) direction than in the surface-consistent direction (orange trajectories), unlike the PP data in Figures 25 and 26, which are known to be surface-consistent.

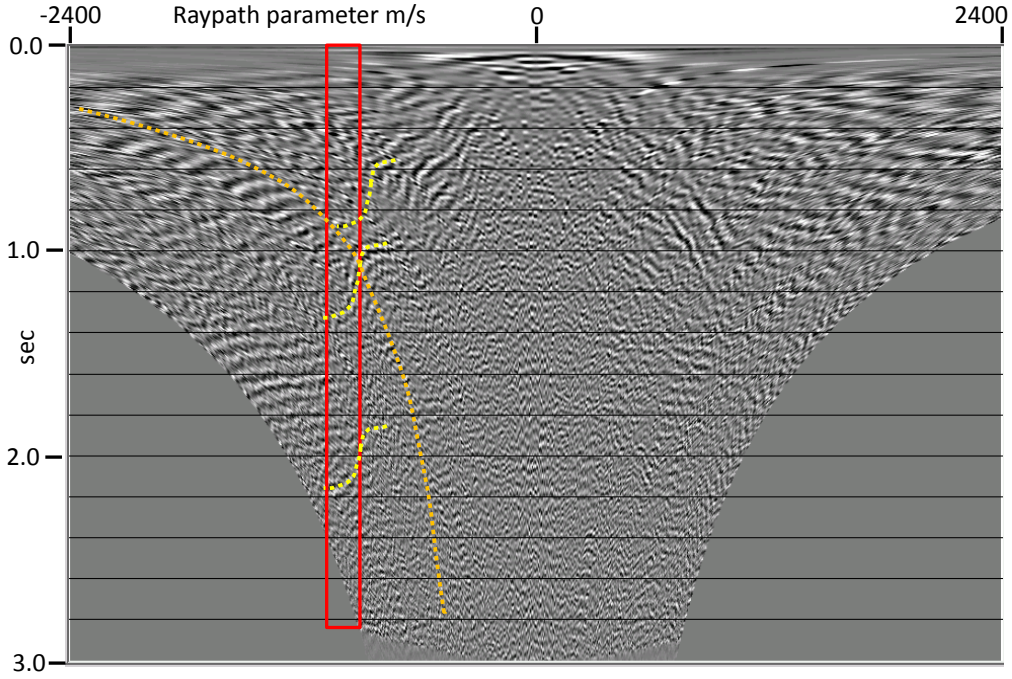

FIG. 34. RT transform of source gather 361 from the Hussar PS data set. Orange trajectory follows an XT trace, red corridor outlines the common-raypath direction, and the yellow contours show some of the large common-raypath statics anomalies and their alignment in this domain.

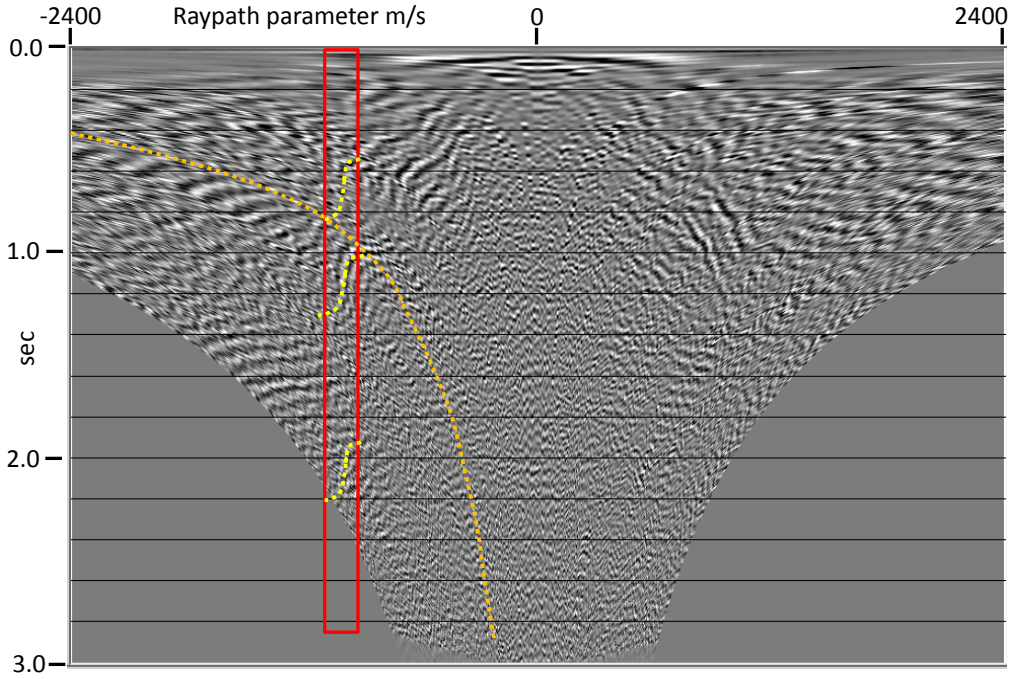

FIG. 35. Snell Ray Transform (linear velocity increase) of source gather 361 from the Hussar PS data set. Orange trajectory follows an XT trace, red corridor outlines the common-raypath direction, and the yellow contours show the improved alignment of statics anomalies in the common-raypath domain.

DISCUSSION

As outlined in the original description of the raypath interferometry technique (Henley, 2012a), The purpose of remapping raw seismic data from source or receiver gathers into the radial trace domain is to allow statics anomalies on various reflection events at different travel times to be analyzed and corrected by grouping them by common near-surface raypath rather than simply by common surface point. In looking closely at our results in the previous section, it appears that most of the benefit of this remapping comes from simply extracting the anomalies from the common-surface-point domain and allowing them to be analyzed and corrected independently. It seems not to be crucial that the anomalies in the new domain align in the common-raypath direction, in order to obtain a very satisfactory solution using raypath interferometry. However, when the data themselves are clearly nonstationary, as in the case of the Hussar PS data set, the common-raypath alignment appears to be more important for a good interferometric solution. In either case, using Snell Ray trajectories, whether created using a velocity function, or a simple linear increase, seems to provide slightly better interferometry solutions than simply using linear RT trajectories, with both shallow and deep reflections showing improved coherence.

For creating the reference wavefield corresponding to each common-raypath parameter gather, the two methods compared here (trace mixing and Eigenvector filtering) provide entirely comparable results. In either case, horizon flattening needs to be applied first, whenever there is structure in any event within the desired image of half the event wavelength or more. In the case of trace mixing, the wavefield estimate is more robust if trim statics are applied to the raw common-raypath-parameter gathers first. While this step can be omitted, the interferometric image converges after fewer iterations when trim statics are used. Trim statics appear to be unnecessary when using Eigenvector Filtering, however, because discarding the more detailed (higher order) eigenimages removes any wavelet smear that occurs from stacking misaligned events. Median mixing to infill gaps and remove ‘steps’ in the re-composed (low-order) eigenimage sum seems to be a necessity, however.

CONCLUSIONS

The general method known as raypath interferometry has been used to successfully correct various sets of model and field seismic data for the effects of near-surface irregularities. It applies two unrelated principles, each of which may be adopted individually: removal of ‘statics’ by cross-correlation and deconvolution rather than trace time-shifting; and derivation and application of nonstationary statics using a simple remapping of the raw seismic data, the Radial Trace Transform. The method was devised to correct seismic data sets which violate the basic assumptions for conventional statics correction, but it is entirely general and can be applied to any seismic data set on which coherent events can be detected in enough strength to create a reference wavefield.

While the basic technique works well enough, we have explored possible enhancements and extensions in this report. We have described an alternate method for creating the reference wavefield which avoids the uncomfortable step of applying trim statics, but requires median mixing to eliminate gaps and breaks in the estimated wavefield. We have also tested the use of the Snell Ray Transform instead of the original

Radial Trace Transform to map the raw data into a common-raypath domain for analysis. In this case, we see mild improvement of the interferometry images. We conclude, nevertheless, that it is less important for the mapping operation to accurately create true common-raypath traces than it is to simply extract the visible statics anomalies on reflection events from the surface-consistent domain, making them available for separate analysis and correction, rather than forcing them to have a common solution.

ACKNOWLEDGEMENTS

The author gratefully acknowledges funding and support from CREWES sponsors and NSERC. Discussions with Raul Cova were of great value, as well as various discussions with CREWES staff and students.

REFERENCES

Bakulin, A. and Calvert, R., 2006, The virtual source method: theory and case study, Geophysics, **71**, S1139-S1150.

Claerbout, J.F., 1975, Slant-stacks and radial traces: Stanford Expl. Project Report, **SEP-5**, 1-12.

Claerbout, J.F., 1985, Imaging the earth's interior: Stanford Expl. Project Report, 216-219.

Cova, R., Henley, D.C., and Innanen, K.A.H., 2014, Making shear wave statics actual statics using radial-trace and tau-pi transforms, CREWES Research Report, **26**.

Cova, R., Henley, D.C., and Innanen, K.A.H., 2013a, Non-stationary shear wave statics in the radial trace domain, CREWES Research Report, **25**.

Cova, R., Henley, D.C., and Innanen, K.A.H., 2013b, An interferometric solution for raypath-consistent shear wave statics, CREWES Research Report, **25**.

Cova, R., Henley, D.C., and Innanen, K.A.H., 2014a, Inverting raypath dependent delay times to compute S-wave velocities in the near surface, CREWES Research Report, **26**.

Cova, R., Henley, D.C., and Innanen, K.A.H., 2014b, Making shear wave statics actual statics using radial-trace and tau-pi transforms, CREWES Research Report, **26**.

Henley, D.C. 2003, Coherent noise attenuation in the radial trace domain, Geophysics, 68, No. 4, pp1408-1416.

Henley, D.C., 2004, A statistical approach to residual statics removal: CREWES Research Report, **16**.

Henley, D.C., 2007, Raypath statics revisited: new images: CREWES Research Report, **19**.

Henley, D.C., and Daley, P.F., 2007, Connecting statics deconvolution and seismic interferometry, CREWES Research Report **19**.

Henley, D.C., 2012a, Interferometric application of static corrections, Geophysics, **77**, No. 1, pp Q1-Q13.

Henley, D.C., 2012b, Interference and the art of static correction: raypath interferometry at Hussar, CREWES Research Report **24**.

Margrave, G.F., Mewhort, L., Phillips, T., Hall, M., Bertram, M., Lawton, D.C., Innanen, K.A.H., Hall, K.W., and Bertram, K.L., 2011, The Hussar Low-Frequency Experiment, CREWES Research Report **23**.

Ottolini, R., 1982, Migration of reflection seismic data in angle-midpoint coordinates: PhD. Thesis, Stanford University.

Yedlin, M., 2012, Private communication.